STRUCTURE-BASED DESIGN AND OPTIMIZATION OF DIPEPTIDYL INHIBITORS OF NOROVIRUS 3CL PROTEASE

A Thesis by

Roxanne Adeline Zuñiga Uy

Bachelor of Science, Wichita State University, 2011

Submitted to the Department of Chemistry
and the faculty of the Graduate School of
Wichita State University
in partial fulfillment of
the requirements for the degree of
Master of Science

July 2014

STRUCTURE-BASED DESIGN AND OPTIMIZATION OF DIPEPTIDYL INHIBITORS OF NOROVIRUS 3CL PROTEASE

The following committee members have examined the final copy of this thesis for form and content, and recommend that it be accepted in partial fulfillment of the requirement for the degree of Master of Science with a major in Chemistry.

William C. Groutas, Committee Chair

James G. Bann, Committee Member

Maojun Gong, Committee Member

Li Yao, Committee Member

DEDICATION

To my family near and far

ACKNOWLEDGMENTS

First and foremost, I wish to express my heartfelt gratitude to Dr. William C. Groutas for his patience, kindness, intelligence, and encouragement. He keeps my passion for learning and perseverance alive.

I would also like to thank my committee members Dr. James Bann, Dr. Maojun Gong and Dr. Li Yao for their support and enthusiasm. I am also very grateful to Dr. David Eichhorn, Susan McCoy, Mary Cambridge, Debbie Mitchum, Laurie Reese, and Marcia Norton for their assistance and guidance in administrative matters.

Sincerest of thanks to Dr. Kyeong-Ok Chang, Dr. Yunjeong Kim, Dr. Gerald H. Lushington, and Dr. Duy Hua for their collaboration in the norovirus project.

I am deeply indebted to my past and present lab mates, Dr. Kevin Alliston, Dr. Sridhar Aravapalli, Dr. Sivakote Mandadapu, Pathum Weerawarna, Anushka Chathuranga Galasiti Kankanamalage, and Chakri Vishnu Damalanka. The lab is so much livelier because of their friendship and support.

I am grateful to my parents, Roberto and Rosario, and my siblings Rachelle Claudine, Rosalynd Ysabelle Rebekah Anne, Reuben Fredrick, and Regina Sallee for never once doubting me. I am especially thankful to The Mission Church, for their never-ending love and constant prayers. I am blessed beyond belief to call them my family here in WSU.

Last, but definitely not least, I am thankful to God. He is my strength, my hope, and my first love.

ABSTRACT

Noroviruses are the primary cause of acute gastroenteritis. They are associated with increased hospitalization and mortality among the elderly and immunocompromised patients. In developing countries, noroviruses are linked to significant mortality (200,000) in children < 5 years old. Importantly, norovirus infection poses a high bioterrorism threat, and the problem is further compounded by the current dearth of effective vaccines or norovirus-specific antivirals.

The studies described in this thesis lay the groundwork for the discovery and development of small molecule therapeutics for the treatment and prophylaxis of norovirus infection. Specifically, these studies have as their primary focus the structure-based design and optimization of a dipeptidyl series of inhibitors of norovirus 3CL protease, an enzyme shown to be essential for replication of the virus and a validated target for the development of anti-norovirus therapeutics. The studies described herein include the synthesis and in vitro biochemical evaluation of dipeptidyl transition state inhibitors and transition state mimics of 3CL protease. The selectivity of the inhibitors, as well as the anti-norovirus activity of the synthesized compounds in a cell-based replicon system was also evaluated.

TABLE OF CONTENTS

Chapter Page

1. INTRODUCTION ……1

1.1. Background on acute gastroenteritis ……...1
1.1.1. Scope of disease …….....1
1.1.2. Difficulties surrounding NoV experimentation ……2
1.2. Norovirus genome …….....3
1.2.1. Norovirus 3CL protease ……..3
1.2.2. X-ray structure ……..4
1.2.3. Substrate specificity ……5
1.3. Mechanism of action of cysteine proteases ……...6
1.4. Protease inhibitors ……..8
1.4.1. Characterizing protease inhibitors ……8
1.4.1.1. Affinity labels ……8
1.4.1.2. Mechanism-based inhibitors ……..9
1.4.1.3. Transition state analogs ……9
1.4.1.4. Non-covalent inhibitors ……10
1.4.2. Classes of non-covalent inhibitors ……11
1.4.2.1. Competitive ……11
1.4.2.2. Uncompetitive ……12
1.4.2.3. Mixed inhibition ……..12
1.5. Enzyme kinetics ……13
1.5.1. Quantitative analysis of enzyme inhibition ……13
1.5.1.1. The Michaelis-Menten constant, K_M ……...13
1.5.1.2. The specificity constant, k_{cat}/K_M ……..14
1.5.1.3. The inhibition constant, K_i ……15
1.5.1.4. The functional strength of inhibitor, IC_{50} ……15
1.5.2. Types of assays ……16
1.5.2.1. Chromogenic assays ……16
1.5.2.2. Fluorometric assays ……..16
1.5.3. Selectivity studies ……..17
1.6. Inhibitors of NoV 3CL protease ……..18
1.7. RESEARCH GOALS ……20

2. STRUCTURE-BASED DESIGN OF INHIBITORS ……21

3. EXPERIMENTAL SECTION ……..27

3.1. Chemistry ……..27
3.1.1. Synthesis of inhibitors ……...27
3.1.2. Biochemical evaluation of inhibitors ……...30

TABLE OF CONTENTS (cont.)

Chapter Page

3.2. Experimental design ……30
3.2.1. Representative synthesis of compounds ……...30
3.2.2. Representative biochemical evaluation ……39
3.2.2.1. Screening ……..40
3.2.2.2. Determination of IC_{50} ……41
3.2.2.3. Tests for selectivity ……41
3.2.2.3.1. Human Neutrophil Elastase (HNE) ……41
3.2.2.3.2. α-Chymotrypsin ……42
3.2.2.3.3. Trypsin ……43
3.2.2.3.4. Thrombin ……44
3.2.2.3.5. Cathepsin B ……45
3.2.2.3.6. Factor X_A ……45
3.2.2.3.7. Plasmin ……46
3.2.2.3.8. Carboxypeptidase A ……..47

4. RESULTS AND DISCUSSION ……..49

4.1. Introduction ……..49
4.2. Synthesis of inhibitors ……..50
4.3. Biochemical studies ……52
4.3.1. Inhibitory activity of compounds towards NoV 3CLpro ……52
4.3.2. Selectivity studies ……..54

5. CONCLUSIONS ……..57

6. FUTURE RESEARCH ……57

REFERENCES ……..58

APPENDICES ……65

A. SIGMOIDAL PLOTS FOR IC_{50} DETERMINATION ……66

B. ^{1}H NMR SPECTRA FOR COMPOUNDS **11a-b** ……..68

C. ^{31}P NMR FOR COMPOUNDS **12a-b** ……70

LIST OF TABLES

Table Page

1.1 Substrate specificity of NoV 3CL protease……...6

1.2 General structures of known inhibitors of NoV 3CL protease ……18

3.1 In vitro and cell based inhibition of **11a-b** and **12a-b** against norovirus ……...53

3.2 Selectivity of **11a-b** against a panel of proteases …….....55

3.3 Selectivity of **12a-b** against a panel of proteases …….....56

LIST OF FIGURES

Figure Page

1.1 Norovirus protease open reading frames (ORFs) …….....3

1.2 X-ray structure of NoV protease showing the two domains ……..4

1.3 Berger and Schecter nomenclature for protease-substrate specificity …….....…….....5

1.4 Transition state analogs versus transition state mimics …….....9

1.5 General structure for a dipeptidyl inhibitor (I) …….....…...20

2.1 Transition state inhibitor interaction with NoV 3CLpro …….....21

2.2 Evolution of the design of inhibitor (III) …….....22

2.3 High-resolution crystal structures of TS inhibitor-enzyme complexes …….....…….....24

2.4 X-ray crystal structure of inhibitor (cap segment shown only) and proximal enzyme backbone residues …….....25

3.1 Schematic diagram of the bioevaluation process the small molecule compounds undergo …….....30

4.1 General structure of transition state inhibitors (a) and transition state mimics (b) …….....……...49

4.2 Possible racemization of the α-C in the aldehyde …….....50

4.3 Possible racemization of hydroxyphosphonate epimers. The (S,S) isomer is the active compound …….....51

LIST OF SCHEMES

Scheme Page

1.1 General mechanism of action of cysteine proteases …….....7

1.2 Simplest enzyme-catalyzed reaction …….....11

1.3 Kinetic scheme for competitive inhibition …….....11

1.4 Kinetic scheme for uncompetitive inhibition …….....12

1.5 Kinetic scheme for mixed inhibition …….....13

2.1 Synthesis of glutamine surrogate (**3**) …….....27

2.2 Synthesis of compounds **11 a-b** …….....28

2.3 Synthesis of compounds **12 a-b** …….....29

LIST OF ABBREVIATIONS

3CLpro	3C-like protease
ADMET	Absorption, Distribution, Metabolism, Excretion, Toxicity
Cbz	Carboxybenzyl
$CDCl_3$	Deuterated chloroform
CDI	Carbonyl diimidazole
Cys	Cysteine
DBU	1,8-Diazabicyclo [5.4.0] undec-7-ene
DCM	Dichloromethane
DIEA	Diisopropyl ethylamine
DMF	Dimethyl formamide
DMSO	Dimethyl sulfoxide
DTT	Dithiothreitol
ED_{50}	Effective dosage
EDCI	1-Ethyl-3-(3-dimethylaminopropyl)carbodiimide
EDTA	Ethylenediaminetetraacetic acid
EI	Enzyme-inhibitor complex
ES	Enzyme-substrate complex
EP	Enzyme-product complex
FUT2	α(1,2)fucosyltransferase
GI	Genogroup I
GII	Genogroup II

LIST OF ABBREVIATIONS (cont.)

GIII	Genogroup III
GIV	Genogroup IV
GV	Genogroup V
Gln	Glutamine
Glu	Glutamic acid
HBGA	Histo-blood group antigen
HCV	Hepatitis C virus
HEPES	4-(2-hydroxyethyl)-1-piperazineethanesulfonic acid
His	Histidine
HNE	Human Neutrophil Elastase
HPLC	High Performance Liquid Chromatography
IC_{50}	Half maximal inhibitory concentration
Kb	Kilo base
kDa	Kilodalton
LiHMDS	Lithium hexamethyldisilazane salt
NHMec	7-amino-4-methylcoumarin
NMR	Nuclear Magnetic Resonance
NoV	Norovirus
ORF	Open Reading Frame
PK	Pharmacokinetic
pNA	p-Nitroaniline
RdRP	RNA-dependent RNA polymerase

LIST OF ABBREVIATIONS (cont.)

SAR	Sructure-Activity Relationship
TEA	Triethylamine
TFA	Trifluoroacetic acid
THF	Tetrahydrofuran
TLC	Thin layer chromatography
UV	Ultraviolet
VP	Viral protein
VPg	Viral protein-genome linked

CHAPTER 1
INTRODUCTION

1.1 Background on Acute Gatroenteritis

1.1.1 Scope of disease

There are 31 major pathogens in the United States that cause 9.4 million episodes of waterborne and foodborne illnesses and over 1000 fatalities, annually. NoroVirus (NoV) is the leading cause of foodborne diseases and accounts for more than 50% of infections, 26% of hospitalizations, and 11% deaths [1]. Gastroenteritis, more commonly known as stomach flu, is an inflammation of the lining of the intestines, which results in diarrhea, nausea, vomiting, stomach pain, fever, headaches, and body aches [2]. NoV accounts for more than 90% of all acute gastroenteritis cases. The smaller percentage is as a result of bacterial or parasitic infection [3].

NoV outbreaks are very hard to contain due to the extremely contagious nature of the virus. Hospitals, cruise ships, hotels, day care centers, and any closed setting are susceptible to NoV outbreaks [3, 4]. Transmission of the virus may be direct (person-to-person) or indirect (surface-to-person) [5]. Since NoV is very stable, it is able to stay on surfaces for an extended period of time and still be viable. The most effective prevention of NoV infection is proper hand washing procedures. Alcohol based sanitizers are becoming popular in many locations, however, their effect on disinfecting NoV seems to be minimal [6].

NoVs possess characteristics that expedite the spread in epidemics. First of all, NoVs are exceptionally stable. They are stable in the temperature range of 0 to 60°C and are able to withstand high concentrations of chlorine [7]. Even if most of the virions

pass away in the said conditions, NoV has a low infectious dose. Less than 10 viral particles are needed for a host to be infected [8]. Prolonged duration of viral shedding also increases the risk of secondary spread [9]. Finally, there is a lack of complete cross-protection against the various NoV strains and limited long-term immunity in the human population, so the risk of repeated infections is remarkably high [10].

1.1.2 Difficulties surrounding NoV experimentation

Currently, there are no known effective vaccines or antiviral agents on the market. There are multiple factors that contribute to the difficulty of developing drugs against NoV, one of which is the considerable number of strains of NoV [1, 11]. Efficacy of a potential drug against one strain does not necessarily guarantee protection from another strain. In other words, there is no cross protection among the different NoV strains. Another issue is the lack of capability to culture human NoV in immortalized cells [12]. Most of the studies done in NoV are done in volunteer studies [13], human NoV replicons [14], and murine NoV systems [15]. Lastly, the NoV life cycle is yet to be fully understood due to the lack of human NoV cultures, therefore, direct serotyping using neutralizing antibodies is not possible [16].

There is a percentage of persons that seem to be immune to norovirus infection. In a volunteer study, 29% of the participants did not develop an illness regardless of the dose of the NoV challenge introduced. This population is recessive for the α(1,2)fucosyltransferase (FUT2) gene in the ABH histo-blood group antigen (HBGA) family [5]. The FUT2 gene is responsible for the production of H type-1 oligosaccharide ligand required for NoV binding. Individuals with this deficiency are naturally immune to NoV. However, some individuals who are not recessive to FUT2 still show some

protection against NoV, suggesting a multifactorial resistance. There may be a memory immune response or some still unidentified reason for the unexpected innate immunity.

1.2 Norovirus genome

1.2.1 Norovirus 3CL protease

NoV is a member of the *Caliciviridae* family [17]. It has a single strand, positive-sense 7-8 kb RNA genome that determines the production of a polyprotein precursor. This precursor is processed by virus-encoded viral main protease, also known as 3C-like cysteine protease (3CLpro), which is essential for viral replication [18]. Their replication utilizes an error prone mechanism, resulting in a high degree of diversity [19]. The high diversity of this virus makes the search for therapeutics all the more challenging. NoV is divided into five genogroups (GI to GV), however, only GI, GII, and GIV cause disease in humans [3].

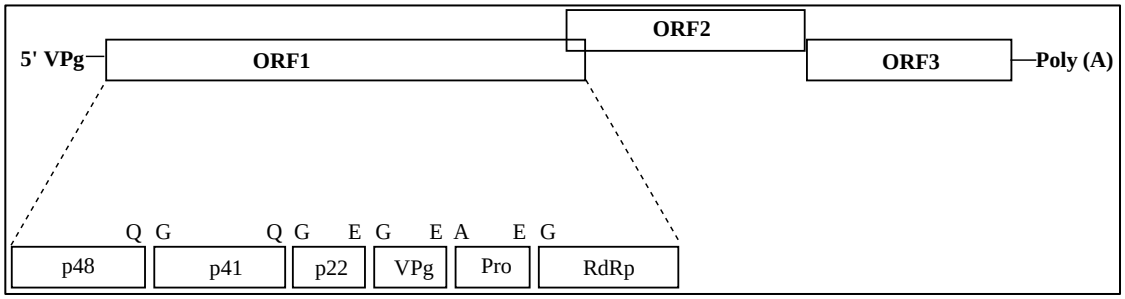

Figure 1.1: Norovirus protease open reading frames (ORFs)

An open reading frame (ORF) is a part of the genome that does not contain stop codons and encodes for various proteins. NoV consists of three ORFs: ORF1, ORF2, and ORF3 (Figure 1.1) [5, 20]. ORF1 encodes the nonstructural protein, a large polyprotein that is processed into six mature products by the viral 3C-like protease: p48 (N-terminal protein), p41 (an NTPase), p22 (a 3A-like protein), a Vpg protein, the 3CL protease, and RdRP (RNA-dependent RNA polymerase) [18, 21]. ORF2 encodes a

capsid protein containing 180 molecules that form a regular icosahedral virion [22]. Lastly, ORF3 encodes a small basic protein [23]. 3C-like protease is essential to the processing of ORF1 polyprotein by catalyzing the cleavage mechanism and is a factor in cellular translation inhibition.

1.2.2. X-ray structure

NoV 3CL pro is responsible for the cleavages of viral polyprotein into intermediate or mature virus proteins [24]. It exhibits a chymotrypsin-like fold, which consists of two domains connected by a large loop. The active site of the protease is found in a depression on the enzyme's surface between domains one and two (Figure 1.2). The substrate specificity of a protease is dictated by the contiguous amino acids to the site where peptide hydrolysis takes place [20, 25].

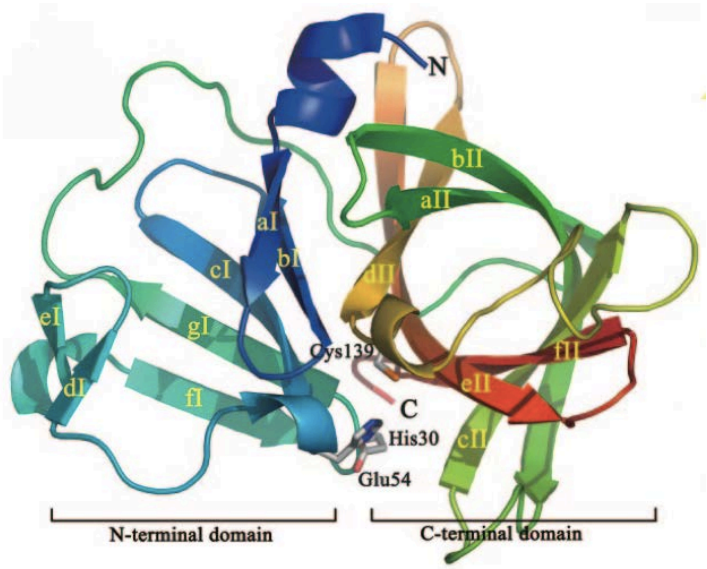

Figure 1.2: X-ray crystal structure of NoV protease showing the two domains

Domain I is responsible for a number of interactions with the active site ligand. It consists of a short N-terminal two-turn α-helical region that leads immediately into the first of five β-strands, βaI to βeI. These five β-strands constitute a twisted antiparallel β-

sheet. Domain II is significantly larger in size than the first domain. It is composed of six β-strands, βaII to βfII, that form an antiparallel β-barrel. Domain II constitutes most of the interactions with the active site ligand. In fact, Cys 139, the active site cysteine residue, is found in a large loop linking βcII and βdII [26].

1.2.3 Substrate specificity

Berger and Schechter [27] developed a simple nomenclature for substrate (or inhibitor) residues and their complementary enzyme binding sites. Subsites that bind residues on the N-terminus side of the substrate (non-primed sites) are numbered as S_1 – S_n and those toward the C-terminus (primed sites) S_1' – S_n', beginning from the sites on each

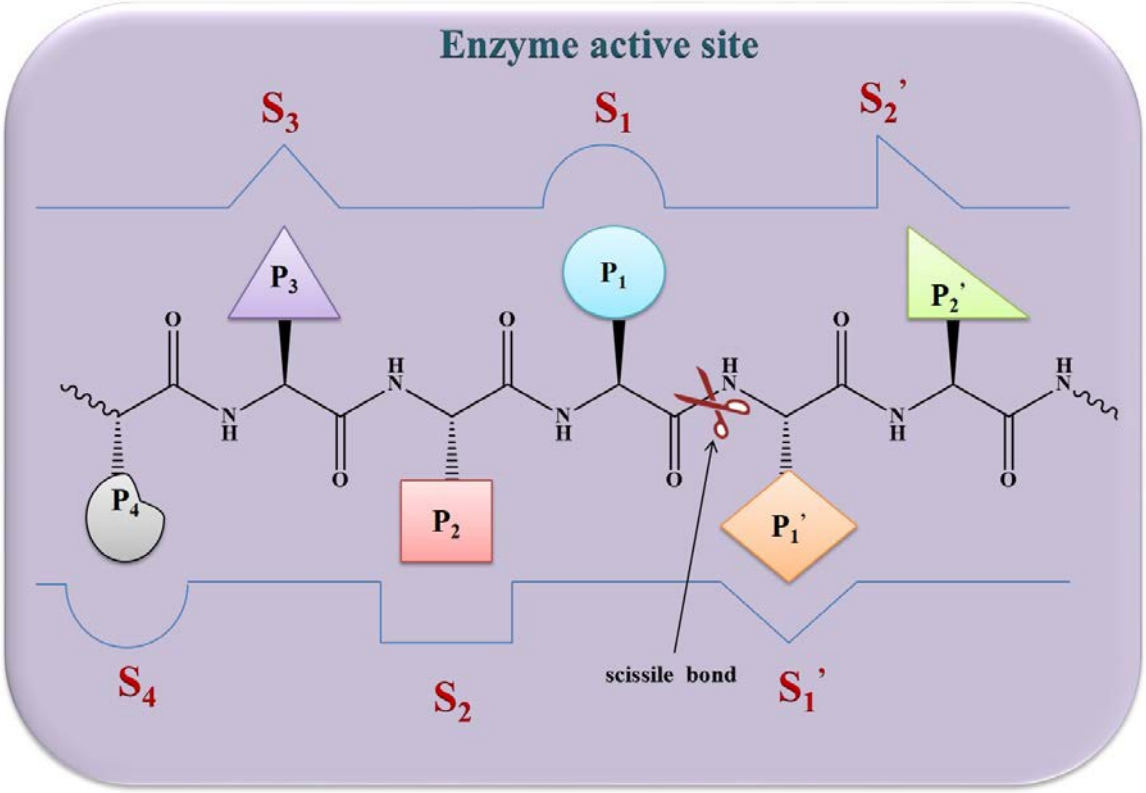

Figure 1.3: Berger and Schecter nomenclature for protease-substrate specificity

side of the scissile bond. The corresponding substrate (or inhibitor) residues are numbered P_1 – P_n and P_1' – P_n', as shown below (see also Figure 1.3). The bond that is cleaved by the protease (the scissile bond) is denoted by the asterisk and P_1 designates the primary substrate specificity residue [27].

Substrate: Pn … – P_3 – P_2 – P_1 * P_1' – P_2' – P_3' – … Pn'

Enzyme: En … – S_3 – S_2 – S_1 – S_1' – S_2' – S_3' – … Sn'

Previous studies with NoV 3CLpro have shown that the enzyme shows a strong preference for Gln-Gly residues at the scissile (P_1-P_1') bond [25]. Furthermore, the residues on adjacent sites show specificity for Asp/Glu-Phe/Tyr-X-Leu (where X= His, Gln or Glu) at the P_5-P_4-P_3-P_2 positions and P at the P_2' position (Table 1.1) [26].

Table 1.1

Substrate specificity of NoV 3CL protease

S5	S4	S3	S2	S1	S1'	S2'
P5	P4	P3	P2	P1	P1'	P2'
D / E	F / Y	H / Q / E	L	Q	G	P

1.3. Mechanism of action of cysteine proteases

The catalytic site provides insight into the properties of the enzyme as a whole [28]. Proteolytic enzymes are grouped together based on the properties of their active sites. Currently, there are five different classes of peptidases: serine, cysteine, aspartic, metallo-, and threonine [29]. NoV 3CLpro is a cysteine endoprotease with a chymotrypsin-like fold, a Cys139-His30-Glu54 catalytic triad, an extended binding site, and a primary substrate for a P_1 residue [30, 31]. NoV 3CL pro, like all proteases, accommodates a 2-6 amino acid sequence in a β-strand conformation. A β-strand is a

linear or saw-toothed arrangement of amino acids in which the amide bonds are almost coplanar and the side chains alternate above and below the plane of the peptide backbone [20, 32].

The general mechanism of action of cysteine proteases is illustrated in Scheme 1.1 below. The cysteine protease contains a thiol (-SH) group (Cys139) that loses a proton to His 30 (general base-general acid catalysis). The resulting thiolate ion is highly nucleophilic and attacks the carbonyl carbon of the scissile bond in the bound substrate to form the first tetrahedral intermediate. The acylation step is completed as

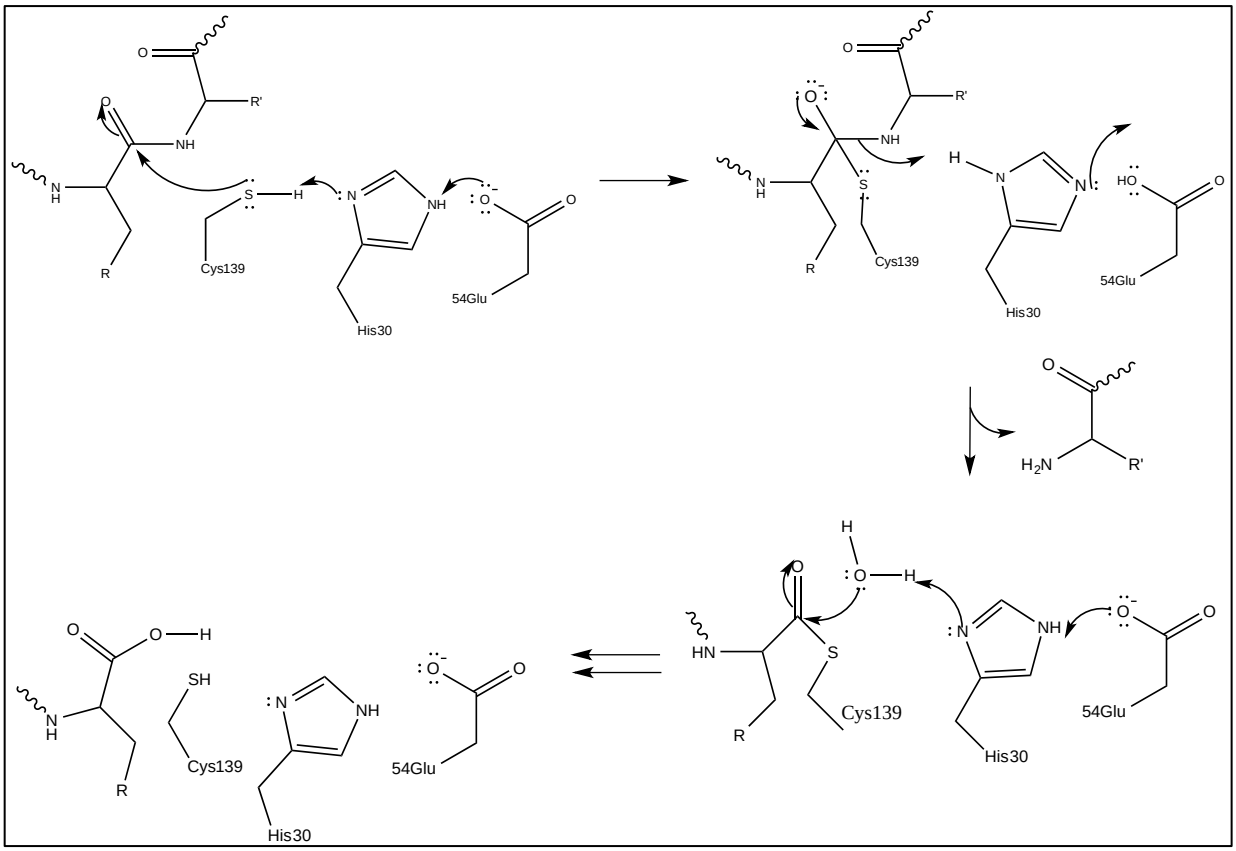

Scheme 1.1: General mechanism of action of cysteine proteases

the electrons on the oxygen come back to reform the C=O bond and the C-N bond is broken. Cleavage of the scissile bond leads to the formation of an acyl-enzyme

intermediate (acylation step). The carbonyl carbon atom is attacked a second time by a nearby H_2O molecule, thus forming the second tetrahedral intermediate. Again, the electrons on the oxygen return to re-form the C=O bond and release the sulfur atom, returning the enzyme to its free (active) state (deacylation).

1.4. Protease inhibitors

A protease inhibitor is defined as any compound that decreases the measured rate of enzyme-catalyzed hydrolysis of a given substrate, either by influencing the substrate binding or the turnover number. The turnover number is the number of reaction processes that each active site catalyzes in a certain unit of time [33].

1.4.1 Characterizing protease inhibitors

There are several ways of characterizing protease inhibitors. The first category is based on the inhibitor's structural layout: protein-based, peptide-based, or low molecular weight inhibitors. The second category focuses on their inhibitory kinetics. Thus, inhibitors can be either reversible or irreversible. Irreversible inhibitors bind to the enzyme tightly via the formation of a covalent bond, such that the enzyme is altered permanently and ceases to function. Reversible inhibitors, on the other hand, suppress enzyme activity in such a way that the action is merely temporary and activity may be restored. The third category classifies inhibitors with regards to their mechanism of action. This is the most favored category because the mechanism of action also determines the kinetics behavior during inhibition. This category includes affinity labels (irreversible) (eq. 1.1), mechanism-based (generally irreversible) (eq. 1.2), transition-state analog (reversible), and non-covalent inhibitors [34].

$$E + I \rightleftharpoons EI \longrightarrow E\text{-}I \qquad (1.1)$$

$$E + I \rightleftharpoons EI \rightleftharpoons EI^* \longrightarrow E\text{-}I^* \qquad (1.2)$$

1.4.1.1 Affinity labels

Affinity labels contain a highly reactive group that usually alkylates one of the essential catalytic residues of the enzyme. Affinity labels are generally non-selective because of their high chemical reactivity. As a result of this lack of selectivity, they are associated with off-target effects and are generally too toxic for use in drug development. Affinity labels are primarily used in identifying and describing different proteases as shown in equation (1.1)

1.4.1.2 Mechanism-based inhibitors

Mechanism-based inhibitors (also known as suicide inhibitors) bind to the protease active site (like the substrate) and undergo processing by the catalytic machinery of the enzyme to yield a highly reactive species which, upon further reaction with an active site nucleophilic residue, yields a covalently-modified inactive form of the enzyme, seen above in equation (1.2).

1.4.1.3 Transition state analogs

A transition state analog is a highly effective inhibitor that is based on the principle, first advanced by Linus Pauling, that “an enzyme must bind the altered substrate in the transition state more tightly than it binds the substrate in the ground state” [35]. Thus, transition state analogs, as the name suggests, resemble the transition state in the reaction pathway (Fig 1.4a). It should be noted that even though transition state analogs form a covalent bond with a catalytic residue, there is a dynamic equilibrium between the reactant (inhibitor) and the product (tetrahedral adduct), hence the inhibition is considered to be reversible (Fig 1.4a). In contrast, transition state

mimics mimic the geometry of the tetrahedral adduct formed during the acylation step. Figure 1.4b shows an example of a transition state mimic inhibitor which resembles the geometry (tetrahedral shape) of the tetrahedral adduct formed from the substrate.

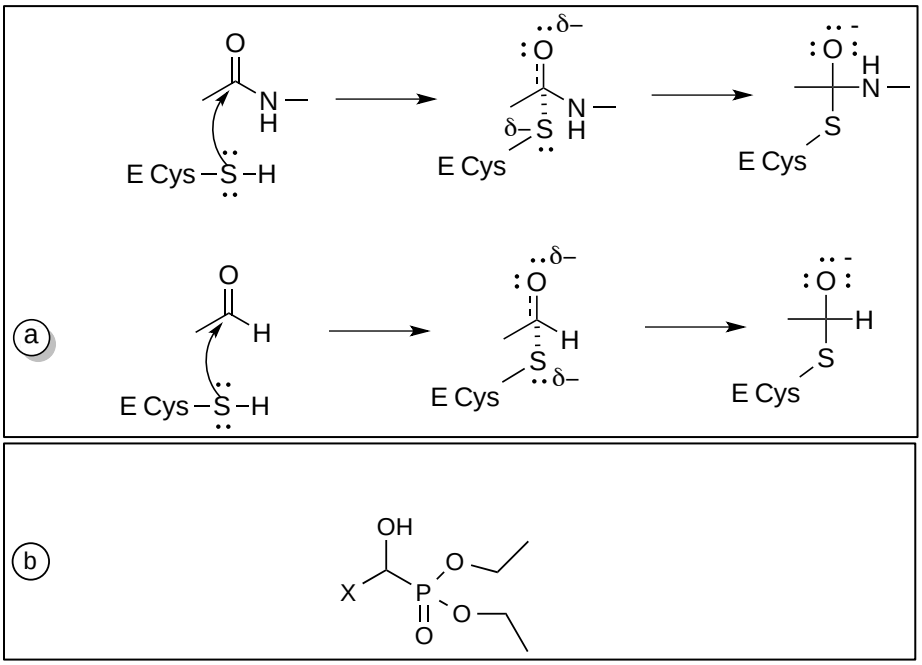

Figure 1.4: Transition state analogs versus transition state mimics

1.4.1.4 Non-covalent inhibitors

Non-covalent inhibitors interact primarily with proteases using ionic, hydrogen bonds, hydrophobic interactions, cation-π interactions, and complementarity instead of covalent molecular forces. Non-covalent inhibitors resemble the substrate of a protease and occupy the active site of the enzyme, resulting in effective inhibition of the enzyme. However, the peptide backbone of such inhibitors is susceptible to attack by many enzymes in the body, especially in the stomach. Further modifications are required to depeptidize the inhibitor to prevent hydrolysis and optimize the ADMET properties of the inhibitor. ADMET is short for adsorption, distribution, metabolism, excretion, and toxicity. These properties are studied and applied to drug candidates and their biochemical

targets to measure their overall efficacy [36]. Non-covalent inhibitors can be divided further into four classes: competitive, uncompetitive, mixed, and non-competitive inhibitors (*vide infra*).

1.4.2. Classes of non-covalent inhibitors

The non-covalent inhibitors mentioned before can be divided further into four classes: competitive, uncompetitive, mixed, and non-competitive inhibitors. The next section discusses the different ways a substance can inhibit the simplest enzyme catalyzed reaction (Scheme 1.2) [33].

$$E + S \underset{k_{-1}}{\overset{k_1}{\rightleftharpoons}} ES \xrightarrow{k_2} P + E$$

Scheme 1.2 Simplest enzyme-catalyzed reaction

1.4.2.1 Competitive Inhibition

When the structure of a substance is similar to that of a substrate, it can bind to the enzyme's substrate-binding site. Such a phenomenon is called competitive inhibition

$$\begin{array}{l} E + S \underset{k_{-1}}{\overset{k_1}{\rightleftharpoons}} ES \underset{}{\overset{k_2}{\rightleftharpoons}} P + E \\ + \\ I \\ K_I \updownarrow \\ EI + S \longrightarrow \text{NO REACTION} \end{array}$$

Scheme 1.3 Kinetic scheme for competitive inhibition

because the substance and the substrate are competing for the same active site. An inhibitor is a successful competitor when it resembles the substrate's structure but is

different enough so that it cannot react the same way as the substrate does (Scheme 1.3). Competitive inhibition can be overcome by increasing the substrate concentration.

1.4.2.2 Uncompetitive Inhibition

Uncompetititve inhibition occurs when a substrate inhibits the ES complex, forming ESI. Uncompetitive inhibitors need not resemble the substrate as it does not bind in the same enzyme active site. Uncompetitive inhibition is significant only for multisubstrate enzymes. Presumably, it reacts with the enzyme after the substrate has bound to the enzyme and distorts the enzyme in such a way that it is rendered catalytically inactive. Uncompetitive inhibition is significant only for multisubstrate enzymes.

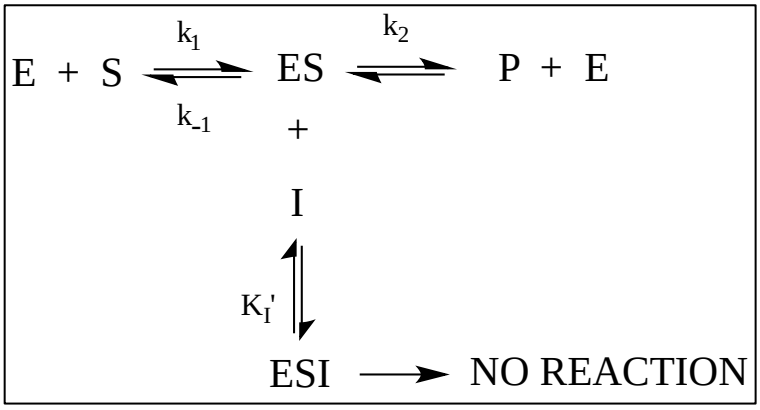

Scheme 1.4 Kinetic scheme for uncompetitive inhibition

1.4.2.3 Mixed Inhibition

A substance that binds both to the free enzyme and ES complex participates in what is known as mixed inhibition. The substance presumably binds to enzyme sites that participate both in substrate binding and catalysis. Scheme 1.5 describes the two possibilities for mixed inhibition. Pure noncompetitive inhibition occurs when the substrate binds the free enzyme and ES complex at an equal rate [33].

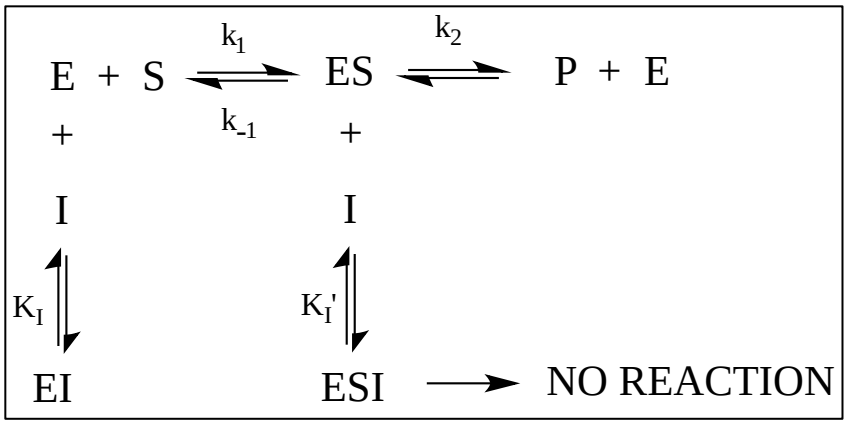

Scheme 1.5 Kinetic scheme for mixed inhibition

1.5. Enzyme kinetics

1.5.1. Quantitative analysis of enzyme inhibition

It is crucial to quantitatively determine the efficiency with which a compound inhibits a protease. Quantitative analysis aids in the understanding of the inhibitor's potency, mechanism of action, and usefulness. Enzyme assay experiments measure the rate of reaction and how the rate changes with varying assay conditions. Results from assay experiments reveal the reaction pathway and thus suggest possible mechanism of action. Kinetics data, as well as detailed information of an enzyme's structure and catalytic mechanisms, furnish valuable insights into the enzyme's biological function(s) and direction for modification for improved therapeutic effect.

1.5.1.1. The Michaelis-Menten constant, K_m

Reaction kinetics is described by rate equations. The simplest enzyme-catalyzed reaction is shown in Scheme 1.2. The enzyme and substrate participate in a bimolecular reaction with a rate of k_1, forming an enzyme-substrate intermediate, ES. The ES complex undergoes a structural rearrangement with a rate of k_2 to produce an enzyme-

product intermediate, EP. Finally, the product is released and the enzyme is free to catalyze another substrate.

Equation 1.3 is also known as the Michaelis-Menten equation. It operates on the assumption that the ES complex maintains a steady state. The steady state assumption advances the notion that the rate of production of ES must equal rate of consumption over most of the reaction course, namely, the concentration of ES is constant. Enzyme kinetics measurements yield expressions for the overall enzymatic reaction. The Michaelis constant, K_m, measures the substrate concentration at which the reaction velocity is 50%, as shown by the initial velocity equation (eq. 1.3) below.

$$v_0 = k_2\,[ES] = \frac{k_2[E]_T[S]}{K_M + [S]} \tag{1.3}$$

The initial velocity is measured before 10% of the substrate has been converted to the product. Doing so reduces the effects of reversible reactions, inhibition of enzyme by the product, and progressive inactivation of the enzyme, which are factors that may complicate calculations and data interpretation [33].

1.5.1.2 Specificity constant, k_{cat}/K_m

The constant k_{cat} is descriptive of the maximum number of substrate molecules transformed to product molecules per active site per unit time. It is the number of times the enzyme “turns over” substrate to product per unit time; hence, it is called the turnover number. The substrate specificity constant is a ratio of the turnover number and the Michaelis constant, k_{cat}/K_m M^{-1} s^{-1}. This ratio is important for evaluating different substrates and gives insight into the speed of the reaction with a given substrate when

bound to the enzyme and the amount of substrate needed to reach the maximum reaction velocity, V_{max}.

1.5.1.3. The inhibition constant, K_i

The dissociation rate of the EI complex back to the free enzyme and free inhibitor is measured by K_I ($K_I = \frac{[E][I]}{[EI]}$). The K_I measures the efficacy of the inhibitor in impeding catalysis; the smaller the K_I value is, the more potent the inhibitor.

The K_I can be determined experimentally by plotting the double reciprocal of the initial velocity ($v_{0)}$ versus varying substrate concentrations (eq. 1.4). Analyzing the K_I values of competitive inhibitors with different structures provides information about the binding requirements of an enzyme's active site and its catalytic mechanism.

$$\frac{1}{v_0} = \left(\frac{\alpha K_M}{v_{max}}\right)\frac{1}{[S]} + \frac{1}{v_{max}} \tag{1.4}$$

1.5.1.4 Funtional strength of inhibitor, IC_{50}

Another quantitative measure of the efficacy of an inhibitor to impede the activity of a protease is IC_{50} [37]. The IC_{50} is defined as the molar concentration of an inhibitor needed to diminish the activity of a protease to 50%. It is not a direct correlation to affinity, however the two can be related by the Cheng-Prusoff equation (eq. 1.5). IC_{50} values are very much dependent on the assay environment and concentrations of the enzyme and substrate.

$$K_I = \frac{IC_{50}}{1 + \frac{[S]}{K_m}} \tag{1.5}$$

1.5.2. Types of assays

1.5.2.1 Chromogenic assays

Molecular absorption spectroscopy is based on the measurement of the transmittance (T) or the absorbance (A) of assays contained in transparent cuvettes that has a path length b. Beer's law demonstrates a linear relationship between the concentration of an analyte, c, and its absorbance (eq. 1.6), where ε is the molar extinction coefficient

$$A = -\log T = \varepsilon bc \tag{1.6}$$

Known concentrations of the enzyme and inhibitor in an appropriate buffer are mixed in a cuvette. After an incubation period, the necessary substrate is mixed in with the solution and then exposed to a UV radiation to measure the difference in absorbance. Widely-used substrates for this type of characterization are N-acylated peptidyl p-nitroanilides (pNa). When the enzyme processes the substrate, the pNa functional group is released and monitored at 410 nm. The difference in molar absorptivity for p-nitroanilides and p-nitroanilines is 10,000 $M^{-1}cm^{-1}$. For competitive inhibition, the inhibitor and the substrate compete for binding with the same enzyme active site. Thus, a when a potent inhibitor is bound to the active site, there will be no change in absorbance over time, due to the fact that none of the substrate is processed and no pNa is released [34].

1.5.2.2. Fluorometric assays

Fluorescence excitation is generated by the absorption of photons. Fluorescence excited states are extremely short-lived ($<10^{-5}$ s). Electrons in their ground state are

excited to a higher state and after a small amount of time, returns to the ground state and in doing so emits radiation.

Dynamic quenching refers to the nonradioactive energy transfer from an excited species to other molecules; it requires contact between the excited species and the quenching agent. It occurs at the same rate as the two species can diffuse together. The quencher concentration must be high enough to ensure high probability of a collision of the two species during the lifetime of the excited state. Fluorescence is emitted from the sample in all directions, but it most conveniently measured at right angles to the excitation beam. This right angle geometry minimizes the effects of scattering and from the intense source radiation.

In the same way that chromogenic assays are setup, fluorometric assays depend on the difference of output as well. Fluorometric assays rely on the difference of emission values when quenchers are introduced in an assay. The substrates used in fluorometric measurements are derivatives of 2-napththylamine (NHNap) and 7-amino-4-methylcoumarin (NHMec) [34].

1.5.3. Selectivity studies

A lead compound is a drug candidate that is subsequently optimized so that it exhibits optimal pharmacological and pharmaceutical characteristics. Parameters optimized during the lead optimization process, include pharmacological activity, cytotoxicity, genotoxicity, potential adverse effects (such as hERG channel, CYP450 and P-glycoprotein inhibition), as well as selectivity. High selectivity is of paramount importance in the case of inhibitors targeting viral serine proteases because of the large number of human proteases that can also be inhibited. A drug reaction with another

protease may lead to a drug allergy or overt toxicity [36]. Human proteases of particular relevance include the blood coagulation cascade enzymes (thrombin, plasmin, factor Xa), digestive enzymes (trypsin, chymotrypsin, carboxypeptidase A) and others. Cross-reactivity is noteworthy between closely related proteases, but also occurs even between distinct classes of serine, cysteine, and threonine enzymes.

1.6 Inhibitors of NoV 3CL protease

Our research group has been at the forefront of scientific endeavors related to the discovery and development of norovirus small-molecule therapeutics. Seminal

Table 1.2

General structures of known inhibitors of NoV 3CLpro

Cyclic sulfamide derivatives 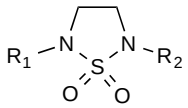	Acyclic sulfamide derivatives 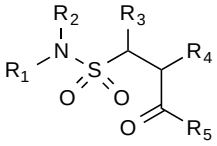
Piperazine derivatives 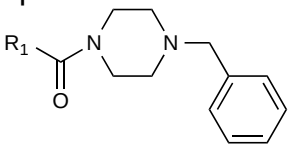	Macrocyclic derivatives 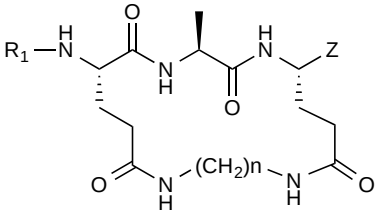
α-hydroxyphosphonate derivatives 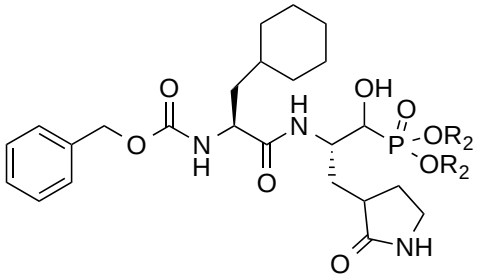	Dipeptidyl derivatives* 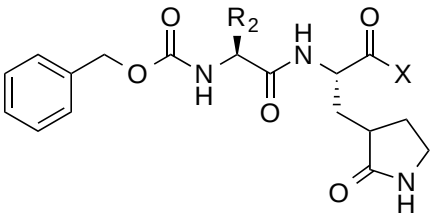

*where x= H, COCONHR, heterocycle, and $NaSO_3$

contributions made in this area of research include the development of the first FRET assay of 3CLpro from GI and GII noroviruses as a screening tool for identifying inhibitors of the 3CLpro, determination of the first high resolution X-ray crystal structures of NoV 3CLpro in complex with peptidyl transition state inhibitors, utilization of a structure-based approach to design the first series of peptidyl and macrocyclic transition state inibitors of the protease, determination of the first solution 3D structure of 3CLpro using high-field NMR, and demonstration for the first time of proof-of-concept using the gnotobiotic pig model of human norovirus infection [38]. Furthermore, these efforts have led to the identification of several classes of inhibitors of 3CLpro, including cyclic and acyclic sulfamides, piperazine derivatives, dipeptidyl and tripeptidyl aldehydes, bisulfite adduct salts, α-ketoamides, α-hydroxyphosphonates, and macrocyclic inhibitors (Table 1.2) [39-49].

These classes of compounds impede the production of non-structural proteins by a polyprotein processed by a virus-encoded 3C-like cysteine protease (3CLpro).

RESEARCH GOALS

During the course of our investigations, inspection of the crystal structure of a dipeptidyl inhibitor (general structure (I), Figure 1.5) revealed that the presence of a 5-membered

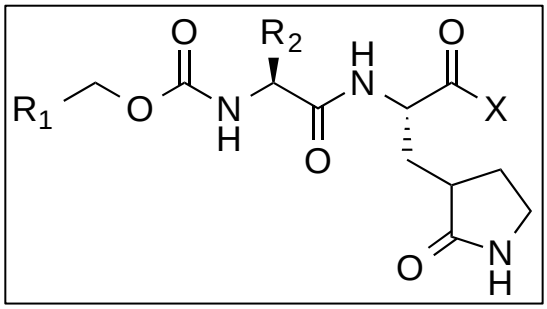

Figure 1.5: General structure for a dipeptidyl inhibitor (I)

aromatic ring at R_1 (the cap), instead of a phenyl or substituted phenyl, would enhance potency. Specifically, it was envisaged that the 5-membered ring could potentially serve as a locus for favorable binding interactions with the backbone of the enzyme. To evaluate this hypothesis, the following research goals were formulated:

a) Structure-based design and synthesis of dipeptidyl transition state inhibitors of NoV 3CL protease that have different 5-membered rings as caps; and
b) In vitro biochemical evaluation of the potency and enzyme selectivity of the synthesized inhibitors.

CHAPTER 2
STRUCTURE-BASED DESIGN OF INHIBITORS

Earlier studies from our laboratory focused initially on the design of transition state inhibitors of NV 3Clpro that incorporate in their structure a recognition element (a peptidyl fragment) that is congruent with the known substrate specificity of the enzyme and a warhead (X=CHO, (C=O)CONHR, $CH(OH)SO_3Na$, α-ketoheterocycle, etc) that interacts with the active site cysteine (Cys139) to form a reversible adduct (Figure 2.1).

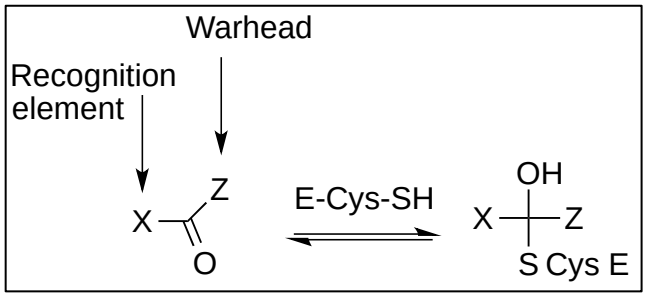

Figure 2.1: Transition state inhibitor interaction with NoV 3CLpro

The lead series, as currently configured, is represented by general structure **(I)** (Figure 2.2). Since the primary specificity residue (P_1) of norovirus 3CLpro is Gln [39], initial design considerations included the use of a glutamine surrogate [50] for optimal synthetic tractability and design flexibility. Thus, the nature of the warhead was investigated by generating a series of peptidyl aldehydes [48], α-ketoamides and α-ketoheterocycles [43] and their corresponding bisulfite adducts [40]. The use of the α-hydroxyphosphonate moiety ($X=CHOH(P=O)(OR)_2$) as a transition state mimic was also investigated [42]. The generated inhibitors were subsequently screened against

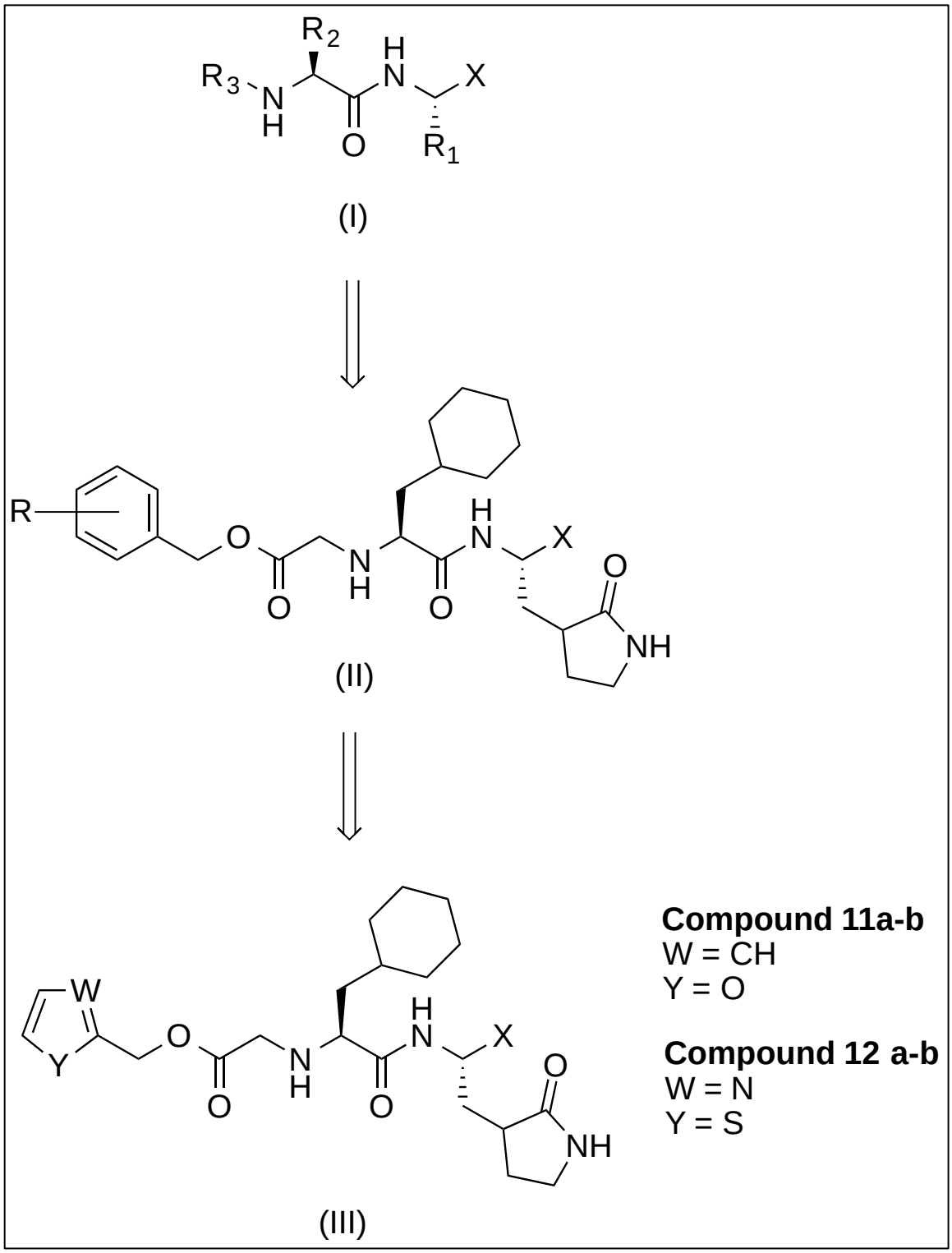

Figure 2.2: Evolution of the design of inhibitor (III).

norovirus 3CLpro and in a cell-based replicon system. Initial SAR (Structure-Activity Relationship) studies in the peptidyl aldehyde series probed the nature of the P_2 residue, since structural studies (*vide infra*) indicated that the Leu side chain did not optimally fill the S_2 pocket [40]. The effect of extending the recognition element (dipeptidyl *versus* tripeptidyl) on potency and cell permeability was also examined [39]. Lastly, because the phenyl ring (Figure 2.2, structure (II)) projects toward the S_3 subsite and beyond, the effect of ring substitution on inhibitory activity was also investigated [43]. Briefly, the results of these early studies demonstrated that (a) the dipeptidyl compounds potently inhibit norovirus 3CLpro *in vitro*, as well as norovirus replication in a cell-based replicon system; (b) a P_2 residue with a R^2 = cyclohexylmethyl side chain is preferred [40]; (c) an array of structurally diverse R groups are tolerated in the α-ketoamide series (X= -(C=O)CONHR), with R = isopropyl or cyclopropyl preferred [43]; (d) tripeptidyl inhibitors showed higher *in vitro* potency, however, they were inactive in the cell-based system, presumably because of poor cellular permeability [39]; (e) the aldehyde and corresponding bisulfite adducts exhibited comparable potency and were found to be generally more potent than the α-ketoamides [40, 43]; (f) high resolution X-ray crystal structures of two dipeptidyl bisulfite salts have been determined [51]; (g) the α-hydroxyphosphonate inhibitors, screened as mixtures of epimers, exhibited noteworthy cellular activity [42]; (h) all compounds showed no nonspecific cytotoxicity up to 500 μM in the cells used for virus replication; and, most importantly, (i) a bisulfite salt adduct of a dipeptidyl aldehyde showed efficacy in the gnotobiotic pig model of norovirus infection and, finally, (j) a meta-chloro substituted α-hydroxyphosphonate inhibitor displayed near optimal pharmacological and physicochemical properties,

including efficacy in a murine model of norovirus infection. This is the first time that dipeptidyl transition state (TS) inhibitors and high-resolution crystal structures of TS inhibitor-enzyme complexes have been reported for norovirus 3CLpro. It is also the first time that bisulfite salt adducts of transition state inhibitors have been shown to inhibit norovirus 3Clpro in vitro, to exhibit anti-norovirus activity in a cell-based replicon system, and to have efficacy in animal models of norovirus infection.

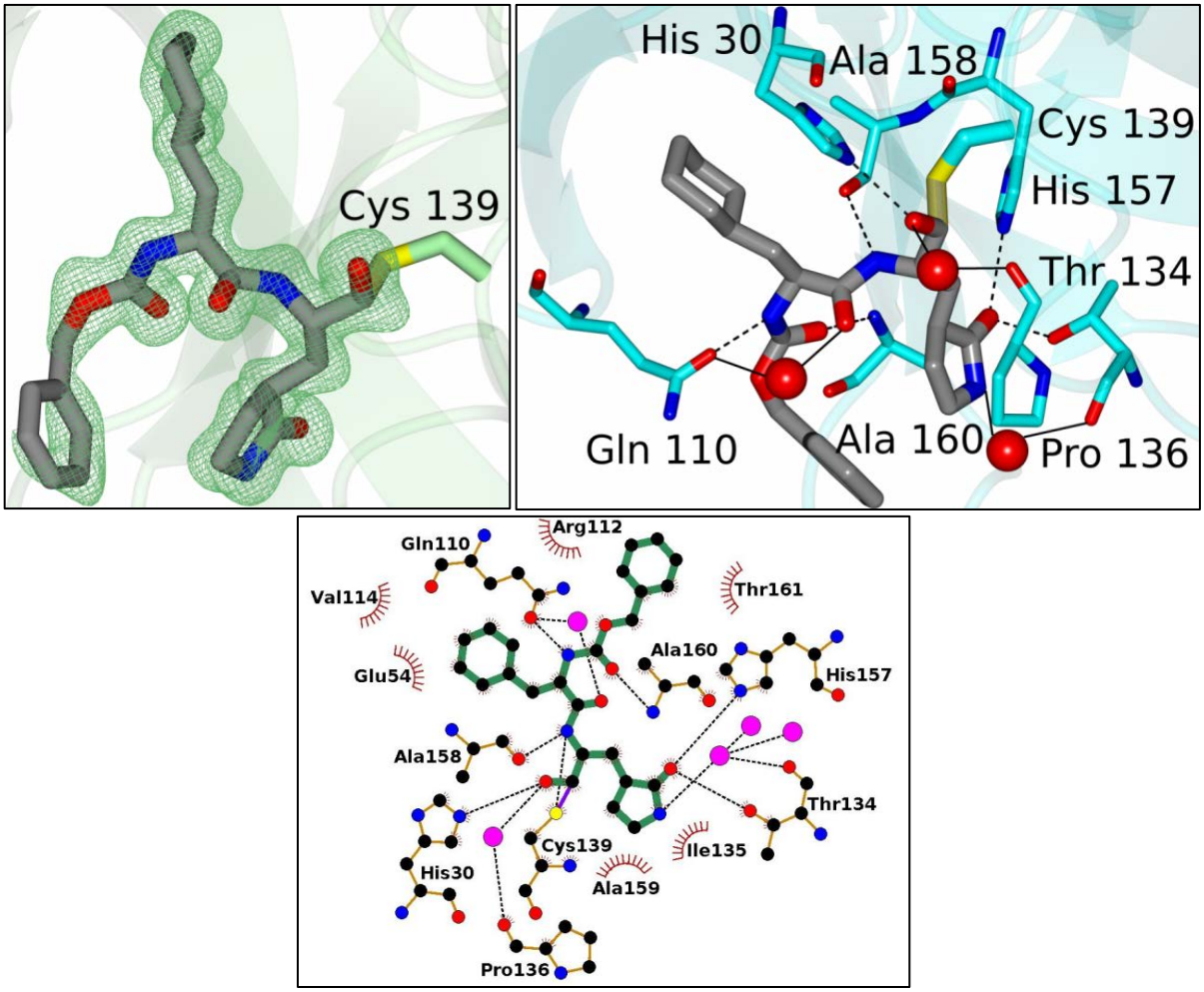

Figure 2.3: High-resolution crystal structures of TS inhibitor-enzyme complexes

Based on the foregoing studies, in order to identify a drug candidate suitable for pre-clinical development, further optimization of potency, enzyme selectivity, ADMET and PK was undertaken by focusing on the structure-based optimization of the “cap”

(Figure 2.2, structure (III)) [52]. “Cap” modifications have been highly successful in improving the potency, selectivity, and pharmacokinetic profiles of HCV NS3/4A protease inhibitors. In order to place the design of the inhibitors on an objective basis, a high resolution co-crystal structure of an inhibitor (structure (I), where R_3 = benzyloxy, R^2 =isobutyl, and X = $CHOH(SO_3^- Na^+)$) was determined, revealing the key binding interactions involved in enzyme-ligand complex (Figure 2.3). On further analysis, the crystal structure revealed opportunities for making additional binding interactions with a more efficient use of chemical structure. Specifically, one such opportunity was recognized by observing that there is a particular stretch of residues spanning Ala159, Ala160, Thr161 and Lys162 that are within 4.0 Å from the benzyl ring (Figure 2.4). In particular, Thr161 and Lys162 are in the closest position. Based on these observations,

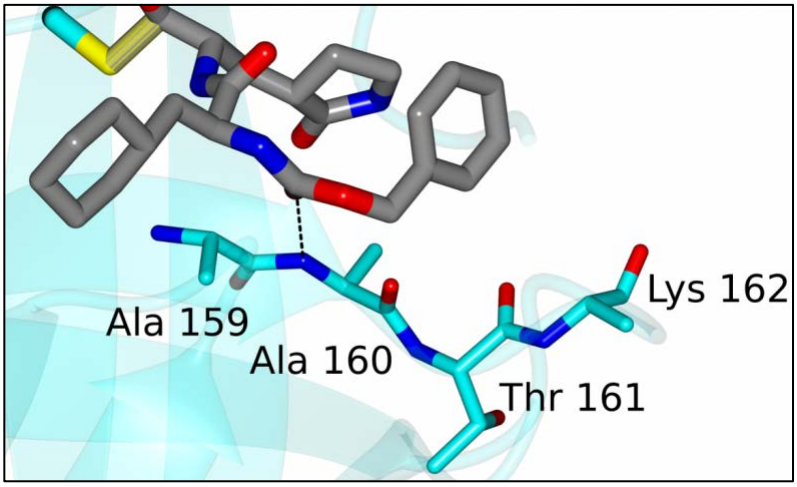

Figure 2.4: X-ray crystal structure of inhibitor (cap segment shown only) and proximal enzyme backbone residues.

we hypothesized that the addition of functional groups (OH, NH_2, CN, F, Cl) at the *ortho* position of the benzyl ring that could potentially function as a hydrogen bond donor or hydrogen bond acceptor to the Thr161 or Lys162 backbone and/or side chains, thereby

stabilizing the flexible benzyl ring, or the replacement of the phenyl ring with a 5-membered ring (as described in this thesis) were predicted to enhance affinity. In the case of a 5-membered ring, computational and docking studies predicted that affinity would follow the order pyrrole>thiophene~furan. Thus, the main thrust of the work described in this thesis was to assess the validity of the aforementioned hypothesis via the synthesis and evaluation of inhibitors represented by general structure (III) (Figure 2.2), where X = CHO (transition state inhibitor) or $CH(OH)(P{=}O)(OR)_2$.

Herein we describe the synthesis and bioevaluation of dipeptidyl transition state analogs and mimics in the in vitro and cell-based replicon system inhibition of NoV 3CLpro.

CHAPTER 3
EXPERIMENTAL SECTION

3.1 Chemistry

3.1.1 Synthesis of inhibitors

The syntheses of dipeptidyl transition state analogs **11a-b** were accomplished according to schemes **3.1** and **3.2**. Aldehyde warheads have proven to be highly effective in inhibiting NoV 3CLpro [53]. The P_1 position is occupied by a Gln surrogate (Scheme **3.1)** which is established as a crucial component of our efforts in developing small molecule therapeutics for norovirus [43]. Lastly, the cyclohexylalanine residue at the P2 position has been shown to participate in hydrophobic interactions with the enzyme and to optimally nestle into the S_2 subsite [40].

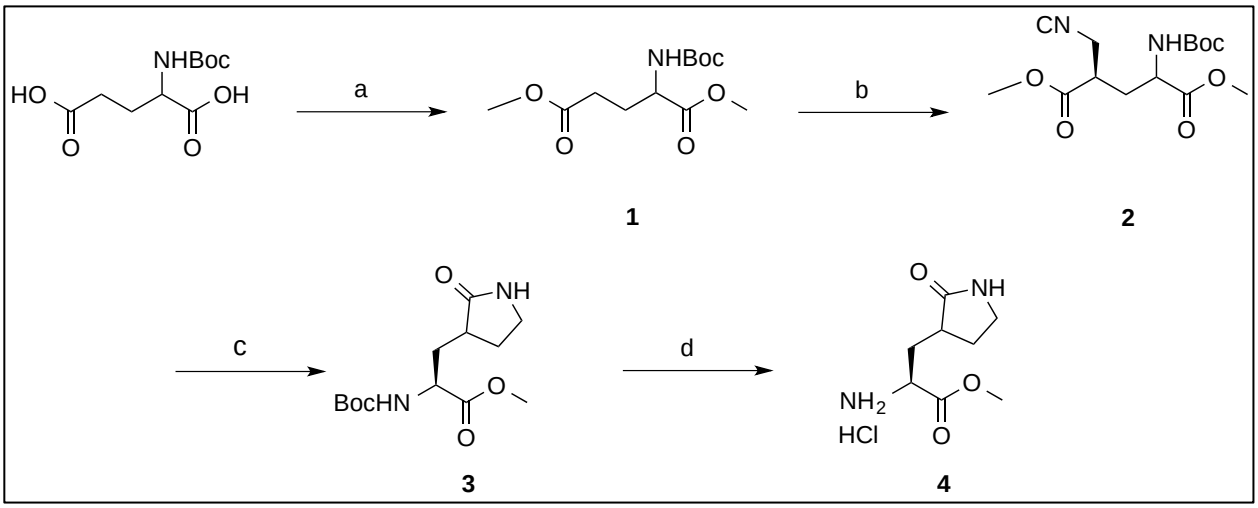

Scheme 3.1: Synthesis of glutamine surrogate (**3**): Reagents and conditions: (a)$NaHCO_3/CH_3I$/DMF; (b) LiHMDS/Bromoacetonitrile/THF; [c]$NaBH_4/CoCl_2/CH_3OH$ (d) 4M HCl / dioxane

Thus, Boc-protected glutamic acid was treated with excess iodomethane in the presence of sodium bicarbonate in dry dimethyl formamide (DMF) to give dimethyl ester, **1**. Compound **1** was then treated with with lithium hexamethyldisilazide (LiHMDS)

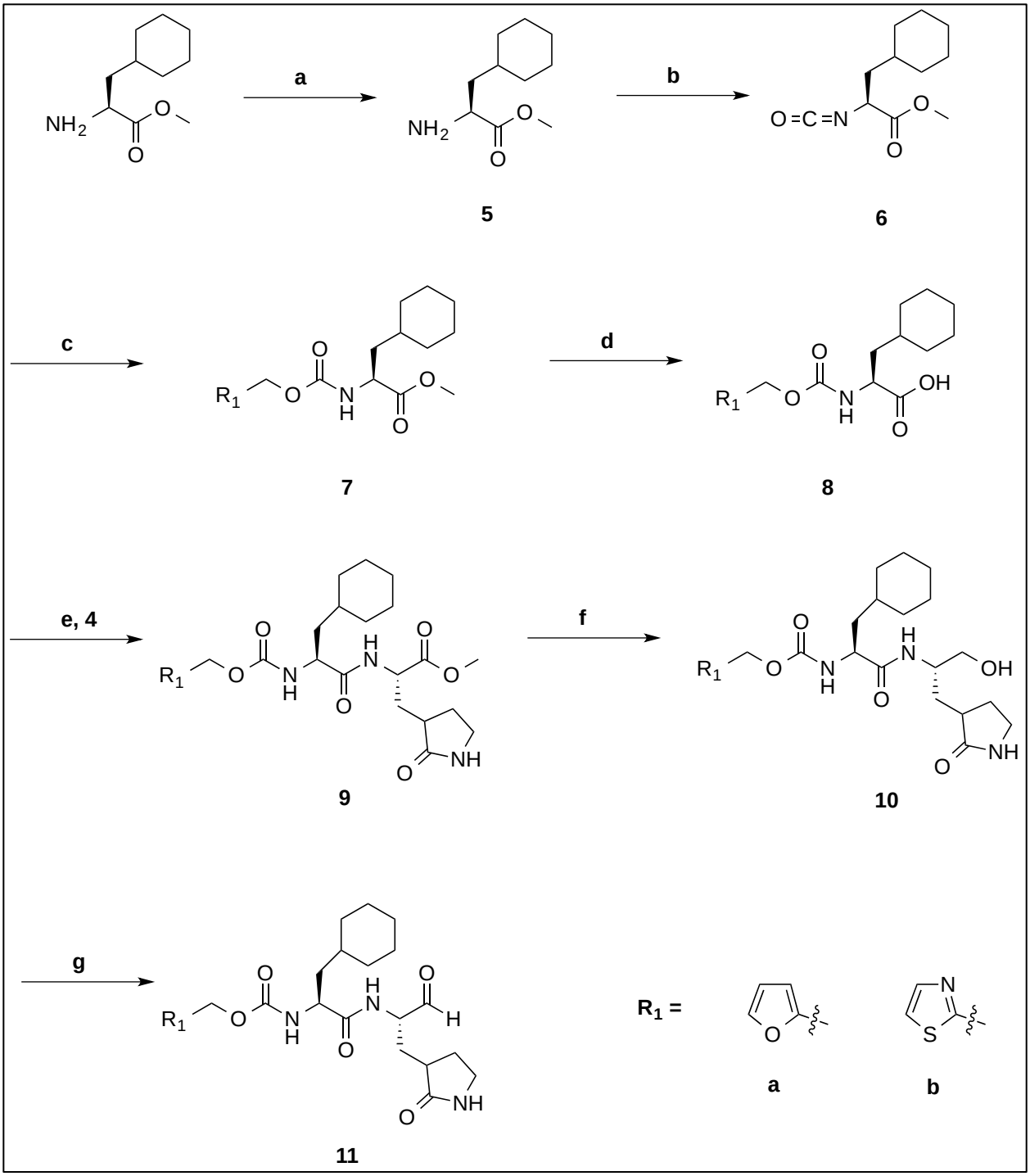

Scheme 3.2 Synthesis of compounds **11 a-b**: Reagents and conditions (a) $SOCl_2/CH_3OH$; (b) $CCl_3O(C{=}O)Cl$/dioxane; (c) R_1OH/TEA; (d) $LiOH/THF/H_2O$; (e) EDCI/HOBt/DIEA/DMF; (f) $LiBH_4$/THF; (g) Dess-Martin periodinane/DCM.

at -78°C in THF followed by the addition of bromoacetonitrile to yield the compound **2.** Reduction of the cyano group with sodium borohydride ($NaBH_4$) in the presence of cobalt chloride hexahydrate ($CoCl_2$•$6H_2O$) in methanol (CH_3OH) yielded the corresponding amine which underwent spontaneous cyclization to give compound **3** [54]. The Boc-protected Gln surrogate was deprotected using dry HCl in dioxane to yield compound **4**, (Scheme **3.1**). β-cyclohexyl-L-alanine was reacted with thionyl chloride ($SOCl_2$) in CH_3OH at 0°C to yield ester **5** which was then refluxed with trichloromethyl chloroformate in dioxane to give the corresponding isocyanate, **6**. The isocyanate was reacted with the appropriate alcohol (R_1-OH) in acetonitrile in the presence of triethylamine (TEA) to give compounds **7a-b**, which were then hydrolyzed with 1M LiOH in THF to produce the corresponding carboxylic acids **8a-b**. The acids were coupled with deprotected glutamine surrogate **4** using 1-ethyl-3-(3-dimethylaminopropyl) carbodiimide (EDCI), hydroxybenzotriazole (HOBt), and N,N-diisopropylethylamine (DIPEA) in dry DMF to give compounds **9a-b**. Esters **9a-b** were reduced to their respective alcohols **10a-b** using lithium borohydride ($LiBH_4$), and then oxidized with Dess-Martin periodinane (DMP) to produce aldehydes, **11a-b** (Scheme **3.2**).

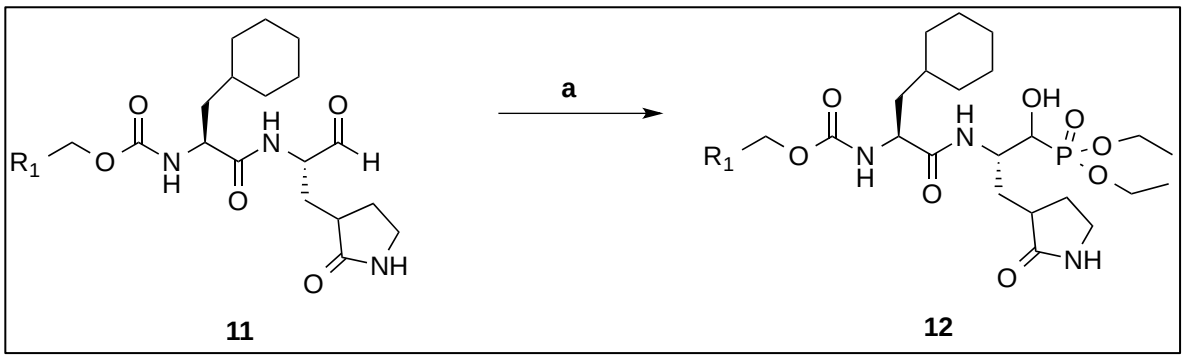

Scheme 3.3 Synthesis of compounds **12a-b**: Reagents and conditions
(a) Diethyl phosphite/DIEA/DCM.

Further reaction of aldehydes **11a-b** with diethyl phosphite and DIPEA in DCM

yielded the corresponding α-hydroxyphosphonate transition mimics (Scheme **3.3**)

3.1.2 Biochemical evaluation of inhibitors

The dipeptidyl aldehydes (compounds **11a-b)** and dipeptidyl hydroxyphosphonates (compounds **12a-b**) were screened for in vitro activity against the norovirus protease enzyme. Compounds that exhibited good potency against the norovirus enzyme at an inhibitor to enzyme ratio of 250 were subjected to further analysis. The IC_{50} values of the "hit" compounds were determined to ascertain their efficacy to impede norovirus activity. Finally, compounds that display desirable IC_{50} values (i.e. nanomolar to low micromolar) were tested for their selectivity against a panel of proteases. This panel consisted of different classes of proteases (serine, cysteine, and metalloproteases) to check for any undesirable inhibitor cross reactivity (Fig 3.1).

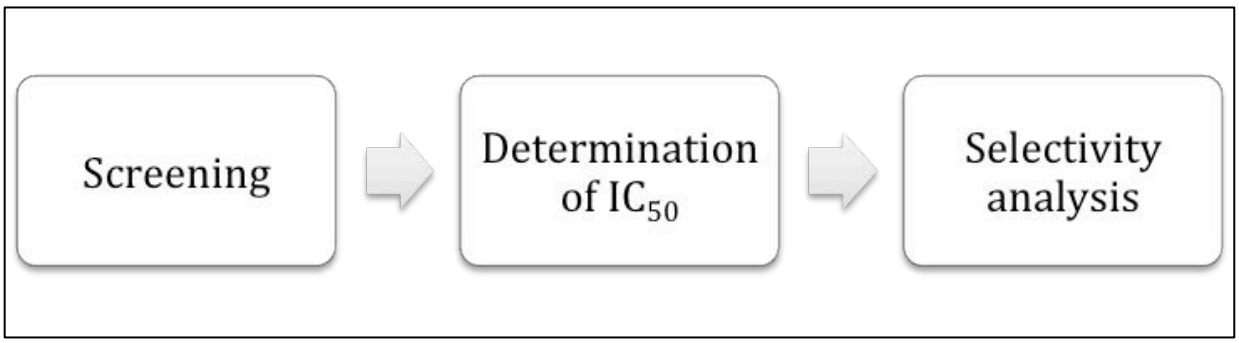

Figure 3.1: Schematic diagram of the bioevaluation process of the small molecule compounds.

3.2 Experimental section

3.2.1 Representative synthesis of compounds

General:

Reagents and solvents were purchased from a variety of chemical suppliers (Sigma-Aldrich, Acros Organics, TCI America, Bachem, and Chem Impex). The ^{1}H and ^{31}P

NMR spectra were recorded using a Varian XL-400 NMR spectrometer. Compound melting points are uncorrected and were determined on a Mel-temp apparatus. Thin-layer chromatography was performed using Analtech silica gel plates to determine the compound purity. The TLC plates of all compounds were eluted using two different solvent systems and visualized with the aid of solid iodine and/or UV light. Each individual compound was identified as a single spot on a TLC plate, with a purity of >95% (as shown by the ^{1}H NMR and HPLC spectra). The 230-450 mesh silica gel used for flash chromatography was purchased from Sorbent Technologies (Atlanta, GA). HPLC data was obtained using Waters 1525 binary HPLC pump with Empower software.

Synthesis of compound 1: N-Boc-L-glutamic acid (61.75 g; 250 mmol) was dissolved in anhydrous DMF (500 mL). Sodium bicarbonate (132.65 g; 1500 mmol) and iodomethane (142.00 g; 1000 mmol) were added sequentially. The reaction mixture was allowed to stir at room temperature for 5 days and the solvent was removed on the vacuum oil pump. The residue was taken up in ethyl acetate (600 mL) and washed with water (1 x 100 mL) and brine (2 x 100 mL). The organic layers were combined, dried over anhydrous sodium sulfate, filtered, and the solvent evaporated on the rotary evaporator, leaving a thick, yellow oil which was purified using flash chromatography to give compound **1** as white crystals. (61.94 g; 90 % yield). ^{1}H NMR ($CDCl_3$): δ 1.41 (s, 9H), 1.90-2.01 (m, 1H), 2.19-2.23 (m, 1H), 2.55-2.69 (m,2H), 3.68 (s, 3H), 3.75 (s, 3H), 4.35 (d, 1H), 5.18 (d, 1H).

Compound 2: A solution of compound **1** (33.01 g; 120 mmol) in anhydrous THF (360 mL) was cooled to -78°C using a dry ice and acetone bath under a nitrogen

atmosphere. A solution of lithium bis(trimethyl silyl) amide (1.0 M solution in THF; 259.2 mL; 259.2 mmol) was added dropwise over a period of 1-2 h. The resulting mixture was stirred for 1 h at -78°C. Bromoacetonitrile (15.4 g; 128.4 mmol) was added dropwise over a period of 1 h while maintaining the temperature below -70°C under N_2 environment. The reaction mixture was stirred at -78°C for 5 h. The reaction was quenched by adding cold CH_3OH (24 mL) in one portion and then stirred for 0.5 h. The resulting methoxide was quenched by adding cold acetic acid (24 mL) in THF (144 mL) in one portion and stirred for an additional 30 minutes. The cooling bath was removed and replaced with a water bath. The reaction mixture was allowed to warm up to room temperature and poured into brine (600 mL). The organic layer was separated and the aqueous layer was extracted with ethyl acetate (2 x 400 mL). The organic layers were combined, dried over anhydrous sulfate, and concentrated on the rotary evaporator, leaving a red oil. The red oil was diluted with DCM (500 mL) and treated with silica gel (50 g) and activated carbon (2-3 scoops). The slurry was filtered using a Hirsch funnel and washed with DCM (50 mL). The yellow filtrate was concentrated on the rotary evaporator, leaving a crude product as a thick yellow oil. The oil was purified using flash chromatography (FC) to give compound **2** as a colorless oil (18.26 g; 49 % yield). ^{1}H NMR ($CDCl_3$): δ 1.45 (s, 9H), 2.11 – 2.23 (m, 2H), 2.79 (s, 2H), 2.82 – 2.91 (m, 1H), 3.73 – 3.79 (m, 6H), 4.34 – 4.45 (q, 1H), 5.11 – 5.21 (d, J = 0.8 Hz, 1H).

Compound 3: Compound **2** (15.72 g; 50 mmol) was dissolved in dry CH_3OH (300 mL). The solution was cooled to 0°C and $CoCl_2$•$6H_2O$ (5.92 g; 25 mmol) was added. The solution turned pink in color. Sodium borohydride ($NaBH_4$) (7.46 g; 200 mmol) was added in portions over 30 min to the stirred solution of compound **2**/methanol/

$CoCl_2$•$6H_2O$. The reaction mixture was stirred for 48 h at room temperature. Most of the CH_3OH was removed using the rotary evaporator, leaving behind a viscous black oil. The black residue was taken up in ethyl acetate (400 mL) and washed with brine (200 mL). The mixture was allowed to settle for 2 h, then 5 % HCl (150 mL) was added to the separatory funnel. The two layers were separated and the aqueous layer was extracted with ethyl acetate (2 x 200 mL). The organic layers were combined and dried over anhydrous Na_2SO_4, filtered, and the solvent was removed on the rotary evaporator, leaving a green oil. The oil was purified using FC to give compound **3** as a white solid. (10.12 g; 71 % yield). ^{1}H NMR ($CDCl_3$): δ 1.40 (s, 9H), 1.79 – 1.93 (m, 2H), 2.09 – 2.18 (m, 1H), 2.42 – 2.52 (m, 2H), 3.30 – 3.39 (m, 2H), 3.75 (s, 3H), 4.27 – 4.35 (m, 1H), 5.44 – 5.51 (d, J = 0.4 Hz, 1H), 5.82 (s, 1H).

Compound 4: Compound **3** (1.43 g; 5 mmol) was dissolved in 4M HCl in dioxane (25 mL) and the solution was stirred for >1 h at room temperature. The completion of the reaction was monitored by the disappearance of the starting material using TLC. The solvent was removed on the rotary evaporator and then the vacuum pump to obtain the product. The resulting product was used in the next step without further purification (1.11 g; 100 % yield). ^{1}H NMR (DMSO): δ 1.59 – 1.71 (m, 1H), 1.85 – 1.93 (m, 1H), 1.97 – 2.08 (m, 1H), 2.23 – 2.31 (m, 1H), 2.55 – 2.62 (m, 1H), 3.14 – 3.23 (m, 2H), 3.75 (s, 3H), 4.12 – 4.24 (m, 1H), 7.98 (s, 1H), 8.58 – 8.68 (s, 3H).

Compound 5: Absolute CH_3OH (60 mL) in a 500 mL round bottom flask (oven dried and purged with N_2) was cooled to 0-5°C using an ice bath. Thionyl chloride (16 mL) was added dropwise to the cooled methanol with stirring. B-Cyclohexyl-L-alanine hydrochloride (41.54 g; 200 mmol) was added to the cold $CH_3OH/SOCl_2$ solution. The

resulting solution was very viscous and off-white in color. The ice bath was replaced with a water bath and the reaction mixture was stirred for 3 h while maintaining the temperature between 45-55°C (air condensing). The resulting solution was a light brown liquid. Most of the solvent was removed on the rotary evaporator, leaving a white solid. The residue was taken up in diethyl ether (300 mL) and filtered using vacuum filtration. The solid was dried over the vacuum pump, to yield compound **5** (43.06 g; 97 % yield). ^{1}H NMR ($CDCl_3$): δ 0.94 – 1.00 (m, 2H), 1.06 – 1.19 (m, 1H), 1.20 – 1.38 (m, 2H), 1.57 – 1.72 (m, 4H), 1.71 – 1.88 (d, J = 0.8 Hz, 3H), 1.89 – 1.99 (m, 1H), 3.79 (s, 3H), 4.04 – 4.11 (t, J = 0.4 Hz, 1H), 8.67 – 8.98 (s, 2H).

Compound 6: Compound **5** (33.26 g; 150 mmol) was placed in a 1 L round bottom flask and dried overnight using a vacuum pump. The flask was flushed with N_2 gas and dry dioxane (500 mL) was added, followed by trichloromethyl chloroformate (44.7 g; 126 mmol), while stirring. The reaction mixture was refluxed for 18 h. The resulting pale yellow solution was allowed to cool to room temperature and the solvent was removed on the rotary evaporator. The residue was vacuum distilled to give a colorless oil, compound **6** (28.4 g; 85 % yield). ^{1}H NMR ($CDCl_3$): δ 0.79 – 0.98 (m, 2H), 1.04 – 1.28 (m, 3H), 1.39 – 1.50 (m, 1H), 1.52 – 1.75 (m, 7H), 3.74 (s, 3H), 3.98 – 4.0 (q, 1H).

Compound 7a: A solution of furfuryl alcohol (0.98 g; 10 mmol) in dry acetonitrile (CH_3CN) (10 mL) was treated with compound **6** (2.11 g; 10 mmol) and TEA (2.5 mL; 10 mmol). The reaction mixture was refluxed for 2 h. The solvent was removed using the rotary evaporator. The residue was diluted with ethyl acetate (75 mL) and then washed with brine (2 x 25 mL). The organic layer was separated and dried over anhydrous sodium sulfate, filtered, then concentrated on the rotary evaporator. The crude product

was purified using FC, giving pure compound **7a** as a pale yellow oil (2.82 g; 92 % yield). ^{1}H NMR ($CDCl_3$): δ 0.83 – 1.00 (m, 2H), 1.09 – 1.28 (m, 2H), 1.28 – 1.39 (m, 1H), 1.44 – 1.55 (m, 1H), 1.60 – 1.74 (d, J = 1.6 Hz, 6H), 1.74 – 1.85 (d, J = 0.8 Hz, 1H), 3.74 (s, 3H), 4.36 – 4.45 (m, 1H), 5.00 – 5.16 (m, 3H), 7.33 – 7.39 (t, J = Hz, 1H), 7.39 – 7.44 (d, J = Hz, 1H), 7.42 (s, 1H).

Compound 7b: Pale yellow oil (3.00 g; 92 % yield). ^{1}H NMR ($CDCl_3$): δ 0.84 – 1.01 (m, 2H), 1.10 – 1.28 (m, 2H), 1.33 – 1.43 (m, 1H), 1.48 – 1.57 (m, 1H), 1.61 – 1.78 (m, 6H), 1.78 – 1.86 (d, J = 0.8 Hz, 1H), 3.71 – 1.78 (d, J = 0.4 Hz, 3H), 4.40 – 4.48 (m, 1H), 5.28 – 5.36 (d, J = 0.4 Hz, 1H), 5.28 – 5.45 (q, 2H), 7.36 – 7.79 (d, J = Hz, 1H), 7.77 – 7.80 (d, J = Hz, 1H).

Compound 8a: A solution of compound **7a** (1.55 g; 5 mmol) in dry THF (20 mL) was treated with 1 M LiOH (17.5 mL) at room temperature and the reaction mixture was stirred for 3 h. The completion of the reaction was monitored by the disappearance of the starting material using TLC. The solvent was removed using the rotary evaporator. Water (10 mL) was added to the residue. The aqueous solution was acidified using ammonium chloride (pH 3~4) and extracted with ethyl acetate (2 x 25 mL). The organic layers were combined, dried with anhydrous sodium sulfate, filtered off, and concentrated on the rotary evaporator. The product, compound **8a**, was a pale yellow solid (1.47 g; 98 % yield). ^{1}H NMR ($CDCl_3$): δ 0.82 – 1.02 (m, 2H), 1.09 – 1.28 (m, 2H), 1.32 – 1.44 (m, 1H), 1.45 – 1.58 (m, 1H), 1.69 – 1.77 (m, 6H), 1.78 – 1.85 (d, J = 0.8 Hz, 1H), 4.36 – 4.44 (m, 1H), 5.00 – 5.15 (m, 3H), 6.34 – 6.38 (m, 1H), 6.39 – 7.43 (m, 1H), 7.42 (s, 1H).

Compound 8b: White solid. (1.32 g; 84 % yield). ^{1}H NMR ($CDCl_3$): δ 0.81 – 1.00 (m, 2H), 1.07 – 1.24 (m, 2H), 1.33 – 1.47 (m, 1H), 1.47 – 1.57 (m, 1H), 1.59 – 1.74 (m, 6H), 1.71 – 1.86 (d, J = 1.2 Hz, 1H), 4.30 – 4.39 (m, 1H), 5.34 – 5.44 (q, 2H), 5.76 – 5.84 (d, J = 0.8 Hz, 2H), 7.32 – 7.36 (d, J = Hz, 1H), 7.74 – 7.80 (d, J = Hz, 1H).

Compound 9a: Compound **8a** (1.48 g; 5 mmol) was dissolved in DMF (10 mL) and EDCI (1.19 g; 6.25 mmol) was added to the stirred solution, followed by HOBt (0.96 g; 6.25 mmol). In a separate round bottom flask, compound **4** (1.11 g; 5 mmol) was dissolved in DMF (7 mL) while kept in an ice bath (temp 0-5°C). DIPEA (2.59 g; 20 mmol) was added to the stirred solution and the reaction mixture was stirred for 20 min. The compound **8a** solution was removed from the ice bath and added to the compound **4** solution and the reaction mixture was allowed to stir at room temperature overnight. The solvent was removed on the vacuum pump and the residue was dissolved in ethyl acetate (1 x 125 mL). The organic layer was washed with sodium bicarbonate (2 x 35 mL) and brine (1 x 35 mL). The organic layer was separated and dried over anhydrous sodium sulfate, filtered, and concentrated on the rotary evaporator, leaving a crude product which was purified using FC. The pure product, compound **9a**, is a white solid (1.3 g; 56 % yield). ^{1}H NMR ($CDCl_3$): δ 0.78 – 1.00 (m, 2H), 1.03 – 1.27 (m, 2H), 1.27 – 1.42 (m, 1H), 1.42 – 1.55 (m, 1H), 1.55 – 1.71 (m, 7H), 1.75 – 1.92 (m, 2H), 2.10 – 2.21 (m, 1H), 2.33 – 2.45 (m, 2H), 3.25 – 3.37 (m, 2H), 3.64 – 3.76 (m, 3H), 4.24 – 4.37 (q, 1H), 4.43 – 4.50 (m, 1H), 4.95 – 5.09 (q, 2H), 5.38 – 5.46 (d, J = 1.2 Hz, 1H), 6.30 – 6.40 (m, 2H), 7.38 (s, 1H), 7.71 – 7.80 (d, J = 0.8 Hz, 1H).

Compound 9b: White solid. (1.44 g, 60 % yield). ^{1}H NMR ($CDCl_3$): δ 0.83 – 1.02 (m, 2H), 1.10 – 1.27 (m, 2H), 1.30 – 1.43 (m, 1H), 1.43 – 1.55 (m, 1H), 1.59 – 1.66 (m, 6H),

1.77 – 1.86 (m, 2H), 2.08 – 2.20 (m, 1H), 2.36 – 2.45 (m, 2H), 3.28 – 3.47 (d, J = 0.8 Hz, 2H), 3.72 (s, 3H), 4.24 – 4.31 (m, 1H), 4.43 – 4.51 (m, 1H), 4.91 – 5.01 (t, J = 1.6 Hz, 2H), 5.20 – 5.27 (d, J = 0.8 Hz, 1H), 5.78 – 5.85 (s, 1H), 6.42 (s, 1H), 7.36 (s, 1H), 7.45 (s, 1H), 7.71 – 7.77 (s, J = 0.8 Hz, 1H).

Compound 10a: A solution of compound **9a** (1.24 g; 2.68 mmol) in dry THF (25 mL) was treated with 2 M $LiBH_4$ (4 mL; 8 mmol) dropwise with stirring. After 15 min, CH_3OH (14 mL) was added to the stirred solution and the reaction was allowed to stir at room temperature overnight. The reaction mixture was cooled in an ice bath and NH_4Cl was added to the solution until the pH was ~ 4. The solvent was removed using the rotary evaporator and the residue was taken up in ethyl acetate (100 mL). The organic layer was washed with brine (1 x 50 mL). The organic layer was separated and the aqueous layer was washed with ethyl acetate (1 x 50 mL). The organic layers were combined, dried over anhydrous sodium sulfate, filtered, and concentrated on the rotary evaporator, to yield compound **10a** as a white solid. (1.06 g, 91 % yield). ^{1}H NMR ($CDCl_3$): δ 0.78 – 1.00 (m, 2H), 1.04 – 1.24 (m, 2H), 1.29 – 1.39 (m, 1H), 1.43 – 1.52 (m, 1H), 1.54 – 1.72 (m, 7H), 174 – 1.86 (m, 2H), 1.91 – 2.01 (m, 1H), 2.33 – 2.48 (m, 2H), 3.26 – 3.38 (m, 2H), 3.52 – 3.70 (m, 2H), 3.92 – 4.01 (m, 1H), 4.16 – 4.24 (m, 1H), 4.98 – 5.08 (m, 2H), 5.30 – 5.37 (d, J = 0.8 Hz, 1H), 5.90 (s, 1H), 6.30 – 6.37 (d, J = Hz, 1H), 6.37 – 6.42 (d, J = Hz, 1H), 7.39 (s, 1H), 7.63 – 7.70 (d, J = 0.8 Hz, 1H).

Compound 10b: White solid. (0.9 g, 75 % yield). ^{1}H NMR ($CDCl_3$): δ 0.83 – 1.00 (m, 2H), 1.07 – 1.23 (m, 2H), 1.27 – 1.38 (m, 1H), 1.41 – 1.52 (m, 1H), 1.76 – 1.88 (m, 6H), 1.90 – 2.0 (m, 1H), 2.33 – 2.47 (m, 2H), 3.27 – 3.36 (d, J = 1.6 Hz, 2H), 3.38 – 3.45 (s, 1H), 3.51 – 3.70 (d, J = 1.6 Hz, 2H), 3.92 – 4.01 (m, 1H), 4.16 – 4.26 (m, 1H), 4.95 (s,

2H), 5.23 – 5.32 (d, J = 0.8 Hz, 1H), 5.83 (s, 1H), 6.41 (s, 1H), 7.37 (s, 1H), 7.45 (s, 1H), 7.68 – 7.76 (d, J = 1.2 Hz, 1H).

Representative syntheses of compounds 11a-b:

Compound 11a: A solution of compound **10a** (1.06 g; 2.43 mmol) in dry DCM (50 mL) was cooled to 0-5°C and stirred for 15 minutes under nitrogen. Dess-Martin periodinane (15.46 g; 5.4 mmol) was added to the stirred solution. The reaction mixture was stirred for 5 min and the ice bath removed. The reaction was allowed to stir for 3 h at room temperature. After the completion of the reaction, 10% $Na_2S_2O_{3(aq)}$ (12 mL) was added and the solution was stirred for another 15 min. The reaction mixture was poured into a separatory funnel. The organic layer was separated and washed with 10% aq $Na_2S_2O_3$ (12 mL), followed by saturated $NaHCO_{3(aq)}$ (2 x 12 mL), water (2 x 12 mL) and brine (1 x 12 mL). The organic layer was dried over anhydrous Na_2SO_4, filtered, and concentrated on the rotary evaporator, to yield aldehyde **11a** as a pale yellow solid (0.73 g, 70 % yield). ^{1}H NMR ($CDCl_3$): δ 0.79 – 1.03 (m, 2H), 1.08 – 1.28 (m, 2H), 1.32 – 1.42 (m, 1H), 1.46 – 1.57 (m, 1H), 1.60 – 1.76 (s, 6H), 1.78 – 1.88 (m, 2H), 1.91 – 2.02 (m, 1H), 2.36 – 2.41 (m, 2H), 3.27 – 3.40 (m, 2H), 4.28 – 4.39 (q, 1H), 5.00- 5.13 (q, 3H), 5.30 – 5.36 (d, J = 0.4 Hz, 1H), 5.96 (s, 1H), 6.32 – 6.43 (d, J = 1.2 Hz, 2H), 7.40 (s, 1H), 8.21 – 8.29 (d, J = 0.4 Hz, 1H), 9.49 (s, 1H).

Compound 11b: Pale yellow solid (0.60 g, 67 % yield). ^{1}H NMR ($CDCl_3$): δ 0.82 – 1.02 (m, 2H), 1.05 – 1.25 (m, 2H), 1.30 – 1.41 (m, 1H), 1.44 – 1.58 (m, 1H), 1.55 – 1.75 (m, 6H), 1.78 – 2.00 (m, 2H), 2.30 – 2.51 (m, 2H), 3.25 – 3.41 (m, 2H), 4.25 – 4.36 (m, 2H), 4.90 – 5.04 (m, 2H), 5.19 – 5.26 (d, J = 0.8 Hz, 1H), 5.79 (s, 1H), 6.41 (s, 1H), 7.37 (s, 1H), 7.46 (s, 1H), 8.23 – 8.30 (d, J = 0.8 Hz, 1H), 9.46 (s, 1H).

Compound 12a: To a solution of compound **11a** (0.22 g; 0.5 mmol) in dry DCM (2.35 mL) was added a solution of diethyl phosphite (0.067 g; 0.5 mmol) in dry DCM (1.69 mL)with stirring, followed by DIPEA (0.189 g; 1.5 mmol). The reaction mixture was stirred for 20 h at room temperature. DCM (15 mL) was added to the reaction mixture and the solution was transferred to a separatory funnel. The organic layer was washed with ammonium chloride (2 x 5 mL) and brine (1 x 5 mL). The organic layer was separated, dried over anhydrous Na_2SO_4, filtered, and concentrated on the rotary evaporator. The crude product was pale yellow oil and purified using FC. Compound **12a** is pale yellow oil. (0.12 g; 42 % yield). ^{1}H NMR ($CDCl_3$): δ 0.79 – 1.00 (m, 2H), 1.08 – 1.26 (m, 2H), 1.26 – 1.55 (m, 6H), 1.40 – 1.56 (m, 2H), 1.55 – 1.73 (s, 6H), 1.73 – 1.87 (m, 2H), 1.96 – 2.04 (m, 1H), 2.32 – 2.52 (m, 2H), 3.25 – 3.36 (m, 2H), 3.53 – 3.68 (m, 1H), 4.08 – 4.22 (m, 1H), 4.22 – 4.34 (m, 1H), 4.91 – 5.11 (m, 2H), 5.94 (s, 1H), 6.19 – 6.32 (d, J = 4.4 Hz, 2H), 7.39 (s, 1H), 7.67 (s, 1H).

Compound 12b: Pale yellow oil (0.071 g; 24 % yield). ^{1}H NMR ($CDCl_3$): δ 0.76 – 0.98 (m, 2H), 1.05 – 1.25 (m, 2H), 1.25 – 1.37 (m, 6H), 1.38 – 1.54 (m, 2H), 1.56 – 1.72 (s, 6H), 1.72 – 1.85 (m, 1H), 1.92 – 2.06 (m, 1H), 2.30 – 2.52 (m, 1H), 3.22 – 3.36 (m, 2H), 3.56 – 3.66 (m, 1H), 4.10 – 4.20 (m, 4H), 4.88 – 5.04 (m, 2H), 5.29 (s, 1H), 5.93 (s, 1H), 6.31 (s, 1H), 7.38 (s, 1H), 7.48 (s, 1H), 7.67 (s, 1H).

3.2.2 Representative biochemical evaluations

General:

Reagents, solvents, and buffer components were purchased from Sigma Aldrich or Fisher Scientific. The UV-vis experiments were performed using Agilent 8453. The FRET studies were executed using HORIBA Fluoromax-4 Spectrophotometer. The

Norovirus 3CLpro enzyme was generously donated by Dr. Kyeong-Ok Chang of Kansas State University. Human neutrophil elastase was purchased from Elastin Products Co. Inc. (Owensville, MO). Plasmin was obtained from Athens Research and Technology (Athens, GA). Factor X_A was acquired from Enzyme Research Laboratories Inc. (South Bend, IN). The cathepsin B substrate (Z-Arg-Arg-pNa) was obtained from Fisher Scientific. The substrate used for the NoV assay (5-Fam-DFHLQGPK(QXLT 520)-OH) was purchased from AnaSpec (Fremont, CA). All other enzymes and substrates were purchased from Sigma Aldrich Corp. (St. Louis, MO).

3.2.2.1 Screening

The norovirus 3CL protease enzyme (6 mg/mL or 3.16 x 10^{-4} M) was received from Dr. Kyeong-Ok Chang of Kansas State University. The enzyme was diluted to 4 x 10^{-6} M using 50 mM NaCl, 0.4 mM EDTA, 50 mM HEPES, pH 8.0. The substrate solution was prepared by dissolving the appropriate amount 5-Fam-DFHLQGPK(QXLT 520)-OH in DMSO to make 5 mM stock solution. The substrate stock solution was diluted to 6 x 10^{-4} M using 50 mM NaCl, 0.4 mM EDTA, 50 mM HEPES, pH 8.0. The inhibitor solutions were prepared by dissolving an appropriate amount of the solid in DMSO to make 2 x 10^{-4} M solution.

To 175 µL of 50 mM NaCl, 0.4 mM EDTA, 50 mM HEPES, 6 mM DTT, 60% glycerol, pH 8.0 assay buffer, 10 µL of 3.5 x 10^{-3} M sample (DMSO for hydrolysis) and 10 µL of 4 x 10^{-6} M NV protease were added. The solutions were mixed and incubated for 30 min. Then 10 µL of 6 x 10^{-4} M of 5-FAM-DFHLQGPK(QXLT 520)-OH substrate solution was added. The solutions were mixed and the samples were run at an excitation and emission wavelengths of 494 nm and 521 nm, respectively, for 10 min at

37.0 °C with a slit width of 1.50 nm [55]. The percent inhibition was calculated by taking the percent difference between the hydrolysis slope and the inhibition slopes. All trials were done in duplicate. The final concentrations were [E] = 2 x 10^{-7} M, [I] = 5 x 10^{-4} M, and [S] = 1 x 10^{-5} M (I/S/E = 250/75/1).

If the percent inhibition of a sample was 100 % at I/E = 250, the concentration of the inhibitor was decreased until the percent inhibition was within 20 to 80 %. Samples that showed promising inhibitory activity (nM or low μM) at the screening stage continued on to the next set of experiments.

3.2.2.2 Determination of IC_{50}

Once a sample was determined to have adequate activity against NoV in vitro, the next step is to ascertain its IC_{50} value. The inhibitor concentration was varied for every run, keeping everything else constant, so that the activity was within the range of 10 to 90 %. The log of the inhibitor concentration was plotted against percent activity. The plot was subjected to a sigmoidal fit. The inhibitor concentration at which the activity was 50 % was recorded as the IC_{50} value [37].

3.2.2.3 Tests for selectivity

3.2.2.3.1 Human Neutrophil Elastase (HNE)

HNE (2 mg) was obtained from Elastin Products Co. Inc. without further purification and was dissolved in 2 mL of 50 mM acetate buffer, 500 mM NaCl pH 5.5. The resulting enzyme solution was diluted (1:10) with the same acetate buffer to yield a concentration of 0.1 mg/mL. The concentration of the active enzyme solution was determined by taking 1000 μL of the 0.02 M substrate solution and adding 33.3 μL of the HNE solution. The assay was run for 60 s at λ = 410 nm, and temperature of 25 °C.

The blank was 1000 µL of the 0.02 M substrate solution and 33.3 µL of the acetate buffer. The resulting absorbances were recorded and the average of three runs was calculated. The molarity of the HNE solution was determined to be 3.077 x 10^{-5} M. The substrate was prepared by dissolving 12 mg of Meo-Suc-Ala-Ala-Pro-Val-pNa is dissolved in 1 mL of 1-methyl-2-pyrrolidinone and then 99 mL of 100 mM Tris-HCl buffer, 500 mM NaCl pH 7.5 to make 0.2 M substrate solution concentration. The inhibitor solutions were prepared by dissolving an appropriate amount of the solid in DMSO to make 3.5 x 10^{-3} M solution.

To 970 µL of 100 mM HEPES, 50 mM NaCl, pH 7.26, 10 µL of 7.7 x 10^{-3} M of inhibitor in DMSO (10 µL of DMSO for the hydrolysis), and 10 µL of 3.077 x 10^{-5} M HNE were added. The solutions were mixed incubated for 30 min. Then 10 µL of 0.07 M MeO-Suc-Ala-Ala-Pro-Val-pNa was added. The solutions were mixed and were run at λ = 410 nm for 120 s at 25 °C. The control solution contained 980 µL of the HEPES buffer and 20 µL of DMSO [56]. The percent inhibition was calculated by taking the percent difference between the hydrolysis slope and the inhibition slopes. All trials were done in duplicate. The final concentrations were [E] = 3.077 x 10^{-7} M, [I] = 7.7 x 10^{-5} M, and [S] = 7 x 10^{-4} M (I/S/E = 250/2275/1).

If the percent inhibition of a sample was 100 % at I/E = 250, the concentration of the inhibitor was decreased until the percent inhibition was within 20 to 80 %.

3.2.2.3.2 α-Chymotrypsin

α-Chymotrypsin from bovine pancreas was obtained from Sigma Aldrich and 10 mg was dissolved in 1 mL of 1 mM HCl. The powder was assumed to be 100 % active with a molecular weight of 25 kDa, therefore the concentration of the enzyme stock

solution was 4 x 10^{-4} M. The enzyme was further diluted (1:2000) with 1 mM HCl to give a final concentration of 2 x 10^{-7} M. The substrate solution was prepared by dissolving Suc-Ala-Ala-Pro-Phe-pNa in DMSO to give a concentration of 4.25 x 10^{-2} M. The inhibitor solutions were prepared by dissolving an appropriate amount of the solid in DMSO to make 2.5 x 10^{-4} M solution.

To 930 µL of 100 mM Tris-HCl buffer, 10 mM $CaCl_2$, pH 7.8, 10 µL of 2.5 x 10^{-4} M of inhibitor (DMSO for hydrolysis) and 50 µL of α-Chymotrypsin were added. The solutions were mixed and incubated for 10 min. Then 10 µL of 4.25 x 10^{-2} M substrate was added. The solutions were mixed and were run at λ = 410 nm for 60 s at 25 °C. The control solution contained 980 µL of the Tris buffer and 20 µL of DMSO [57]. The percent inhibition was calculated by taking the percent difference between the hydrolysis slope and the inhibition slopes. All trials were done in duplicate. The final concentrations were [E] = 1 x 10^{-8} M, [I] = 2.5 x 10^{-6} M, and [S] = 4.25 x 10^{-4} M (I/S/E = 250/42500/1).

3.2.2.3.3 Trypsin

Trypsin from bovine pancreas was obtained from Sigma Aldrich and 1.3 mg of the enzyme was dissolved in 100 mM Tris-HCl , 10 mM $CaCl_2$, pH 7.8. The resulting solution had a concentration of 5 x 10^{-5} M. The substrate solution was prepared by dissolving N-α-benzoyl-L-Arg-pNa in DMSO to give a concentration of 3 x 10^{-2} M. The inhibitor solutions were prepared by dissolving an appropriate amount of the solid in DMSO to make 1.25 x 10^{-2} M solution.

To 970 µL of 25 mM of phosphate buffer, 100 mM NaCl, pH 7.5, 10 µL of 1.25 x 10^{-2} M of inhibitor (DMSO for hydrolysis) and 10 µL of 5 x 10^{-5} M Trypsin were added.

The solutions were mixed and incubated for 10 min. Then 10 µL of 3 x 10^{-2} M substrate was added. The solutions were mixed and were run at λ = 406 nm for 300 s at 25 °C. The control solution contained 980 µL of the phosphate buffer and 20 µL of DMSO [58]. The percent inhibition was calculated by taking the percent difference between the hydrolysis slope and the inhibition slopes. All trials were done in duplicate. The final concentrations were [E] = 5 x 10^{-7} M, [I] = 1.25 x 10^{-4} M, and [S] = 3 x 10^{-4} M (I/S/E = 250/600/1).

3.2.2.3.4 Thrombin

Thrombin from human plasma was obtained from Sigma Aldrich. A vial contained 0.0715 mg of the enzyme and it was dissolved in 1 mL of 25 mM phosphate buffer, 100 mM NaCl, pH 7.5. The resulting solution had a concentration of 1.88 x 10^{-6} M and was further diluted with the phosphate buffer to give a concentration of 1.1 x 10^{-6} M. The substrate solution was prepared by dissolving N-p-tosyl-Gly-Pro-Lys-pNa in DMSO to give a concentration of 2 x 10^{-2} M. The inhibitor solutions were prepared by dissolving an appropriate amount of the solid in DMSO to make 2.75 x 10^{-4} M solution.

To 960 µL of 100 mM of Tris-HCl buffer, 500 mM NaCl, pH 7.5, 10 µL of 2.75 x 10^{-4} M of inhibitor (DMSO for hydrolysis) and 10 µL of 1.1 x 10^{-6} M Thrombin were added. The solutions were mixed and incubated for 30 min. Then 20 µL of 2 x 10^{-2} M substrate was added. The solutions were mixed and were run at λ = 410 nm for 120 s at 25 °C. The control solution contained 970 µL of the phosphate buffer and 30 µL of DMSO [59]. The percent inhibition was calculated by taking the percent difference between the hydrolysis slope and the inhibition slopes. All trials were done in duplicate.

The final concentrations were [E] = 1.1 x 10^{-8} M, [I] = 2.75 x 10^{-6} M, and [S] = 4 x 10^{-4} M (I/S/E = 250/36,363/1).

3.2.2.3.5 Cathepsin B

Cathepsin B from human liver was obtained from Sigma Aldrich. A vial contained 26 µg of the enzyme and it was dissolved in 189 µL of 100 mM acetate buffer, 1 mM EDTA, pH 5.5. The resulting solution had a concentration of 5 x 10^{-6} M. The substrate solution was prepared by dissolving Z-Arg-Arg-pNa in the acetate buffer to give a concentration of 1 x 10^{-2} M. The inhibitor solutions were prepared by dissolving an appropriate amount of the solid in DMSO to make 1.25 x 10^{-3} M solution.

To 96 µL of 100 mM acetate buffer, 1 mM EDTA, 1 mM DTT, pH 5.5, 2 µL of 1.25 x 10^{-3} M of inhibitor (DMSO for hydrolysis) and 2 µL of 5 x 10^{-6} M Cathepsin B were added. The solutions were mixed and incubated for 30 min. Then 2 µL of 1 x 10^{-2} M substrate was added. The solutions were mixed and were run at λ = 410 nm for 200 s at 37 °C [60]. The control solution contained 100 µL of the acetate buffer (with DTT). The percent inhibition was calculated by taking the percent difference between the hydrolysis slope and the inhibition slopes. All trials were done in duplicate. The final concentrations were [E] = 1 x 10^{-7} M, [I] = 2.5 x 10^{-5} M, and [S] = 2 x 10^{-4} M (I/S/E = 250/2000/1).

3.2.2.3.6 Factor X_A

Human Factor X_A solution (1.80 mg/mL in 20 mM Bis Tris, 700 mM NaCl, pH 6.0) was obtained from Enzyme Research Laboratories. The enzyme stock solution (5µL) was diluted with 790 µL cold 100 mM Tris-HCl buffer, 500 mM NaCl, pH 7.5 to make 0.0113 mg/mL. The molecular weight of Human Factor X_A (46,000 kD) was used to

calculate the molar concentration (2.46 x 10^{-7} M). The substrate solution was prepared by dissolving N-p-tosyl-Gly-Pro-Lys-pNa in DMSO to give a concentration of 2 x 10^{-2} M. The inhibitor solutions were prepared by dissolving an appropriate amount of the solid in DMSO to make 2.46 x 10^{-4} M solution.

To 940 µL of 100 mM Tris-HCl buffer, 500 mM NaCl, pH 7.5, 10 µL of 2.46 x 10^{-4} M of inhibitor (DMSO for hydrolysis) and 40 µL of 2.46 x 10^{-7} M Factor X_A were added. The solutions were mixed and incubated for 10 min. Then 10 µL of 2 x 10^{-2} M substrate was added. The solutions were mixed and were run at λ = 410 nm for 300 s at 25 °C [61]. The control solution contained 980 µL of the Tris-HCl buffer and 20 µL of DMSO. The percent inhibition was calculated by taking the percent difference between the hydrolysis slope and the inhibition slopes. All trials were done in duplicate. The final concentrations were [E] = 9.8 x 10^{-9} M, [I] = 2.46 x 10^{-6} M, and [S] = 2 x 10^{-4} M (I/S/E = 250/20,400/1).

3.2.2.3.7 Plasmin

Plasmin from human plasma was obtained from Athens Research and Technology and 1 mg of the enzyme was dissolved in 694 µL of 100 mM Tris-HCl buffer, 500 mM NaCl, pH 7.5 to make 1.44 g/L solution. The enzyme solution was further diluted (1:10) using the Tris-HCl buffer to yield 0.144 g/L. Taking the molecular weight of plasmin as 81,000 kDa, the concentration of the plasma solution was 1.78 x 10^{-6} M. The substrate solution was prepared by dissolving N-p-tosyl-Gly-Pro-Lys-pNa in DMSO to give a concentration of 2 x 10^{-2} M. The inhibitor solutions were prepared by dissolving an appropriate amount of the solid in DMSO to make 4.58 x 10^{-4} M solution.

To 980 µL of 100 mM Tris-HCl buffer, 500 mM NaCl, pH 7.5, 10 µL of 4.58 x 10^{-4} M of inhibitor (DMSO for hydrolysis) and 10 µL of 1.78 x 10^{-6} M Plasmin were added. The solutions were mixed and incubated for 10 min. Then 10 µL of 2 x 10^{-2} M substrate was added. The solutions were mixed and were run at λ = 410 nm for 300 s at 25 °C [62]. The control solution contained 980 µL of the Tris-HCl buffer and 20 µL of DMSO. The percent inhibition was calculated by taking the percent difference between the hydrolysis slope and the inhibition slopes. All trials were done in duplicate. The final concentrations were [E] = 1.78 x 10^{-8} M, [I] = 4.58 x 10^{-6} M, and [S] = 2 x 10^{-4} M (I/S/E = 250/11236/1).

3.2.2.3.8 Carboxypeptidase A

Carboxypeptidase A was obtained from Sigma Aldrich. A vial contained the enzyme solution with a concentration of 5.73 x 10^{-4} M. The enzyme solution was diluted (1:33) using 50 mM Tris-HCl, 500 mM NaCl, pH 7.5 to yield concentration of 1.72 x 10^{-5} M. The substrate solution was prepared by dissolving Hippuryl-L-phenylalanine in DMSO to give a concentration of 3.9 x 10^{-2} M. The inhibitor solutions were prepared by dissolving an appropriate amount of the solid in DMSO to make 4.3 x 10^{-3} M solution.

To 970 µL of 50 mM Tris-HCl buffer, 500 mM NaCl, pH 7.5, 10 µL of 4.3 x 10^{-3} M of inhibitor (DMSO for hydrolysis) and 10 µL of 1.72 x 10^{-5} M Carboxypeptidase A were added. The solutions were mixed and incubated for 5 min. Then 10 µL of 3.9 x 10^{-2} M substrate was added. The solutions were mixed and were run at λ = 254 nm for 60 s at 37 °C. The control solution contained 980 µL of the Tris-HCl buffer and 20 µL of DMSO [63]. The percent inhibition was calculated by taking the percent difference between the hydrolysis slope and the inhibition slopes. All trials were done in duplicate. The final

concentrations were [E] = 1.72 x 10^{-7} M, [I] = 4.3 x 10^{-5} M, and [S] = 3.9 x 10^{-4} M (I/S/E = 250/2267/1).

CHAPTER 4
RESULTS AND DISCUSSION

4.1 Introduction

Gastroenteritis continues to affect millions of people worldwide since effective countermeasures for the viral infections are yet to be reported. There is a pressing need for the discovery and development of small molecule anti-norovirus therapeutics.

Noroviruses belong to the *Caliciviridae* family and contain a single strand, positive sense 7-8 kb RNA genome that encodes a polyprotein precursor that is processed by a virus-encoded 3C-like protease (3CLpro) necessary for virus replication. NoV 3Clpro is classified as a cysteine endoprotease with a catalytic triad (Cys139, His30, and Glu 54) and a substrate specificity of D/E-F-X-L-Q-G-P, where X is H, Q, E, or D at the S_5-S_4-S_3S_2-S_1-S_1'-S_2' pockets. The X-ray crystal structures of NoV 3CLpro, by itself and complexed with a tripeptidyl aldehyde inhibitor, were previously reported [51, 32].

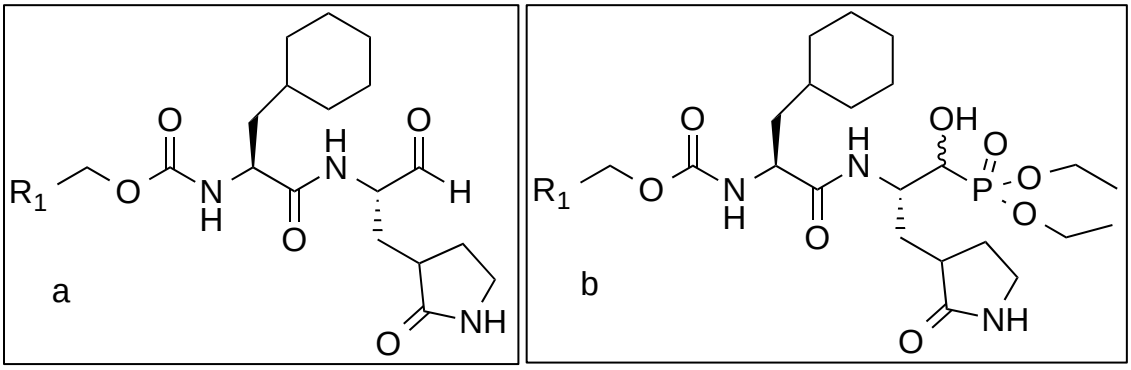

Figure 4.1: General structure of transition state inhibitor (a) and transition state mimic (b)

The primary thrust of the studies described herein was to probe the effect of the "cap" on pharmacological activity, selectivity and physicochemical properties using a

structure-based approach. Specifically, a peptidyl transition state inhibitor (Figure 4.1a) and a peptidyl transition state mimic (Figure 4.1b) were used as representative inhibitors with each inhibitor having a glutamine surrogate occupying the P1 position, since the primary substrate specificity of 3CLpro for the pocket is a glutamine residue [39]. Furthermore, a cyclohexylalanine at the P2 position was also present in the structures of the two inhibitors, since previous studies have shown that the cyclohexyl ring interacts optimally with the hydrophobic S2 subsite of the enzyme. Previously-synthesized series of inhibitors have probed the nature of the R1 group using substituted phenyl or non-aromatic rings. Those studies were carried out without the benefit of a high-resolution enzyme-ligand structure. In the present studies, analysis of the crystal structure of a dipeptidyl inhibitor bound to the enzyme suggested that replacement of the cap with a 5-membered aromatic ring capable of engaging in hydrogen bonding interactions could yield compounds with enhanced pharmacological activity.

4.2 Synthesis of inhibitors

The compounds were synthesized as outlined in Schemes 3.1, 3.2, and 3.3. Syntheses of final compounds **11a**-**b** and **12a-b** were done without any major problems.

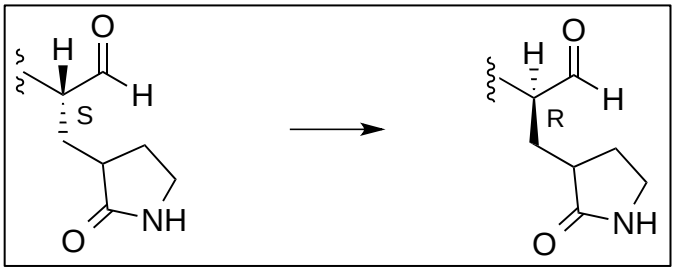

Figure 4.2 Possible racemization of the α-C in the aldehyde

The purification of the aldehydes (compounds **11a**-**b**) was done using FC within two hours in order to prevent racemization at the α-C (Fig 4.2). The ^{1}H NMR spectrum of compound **11a** showed that the isomer ratio is 93.8:6.2 (Appendix B). Compound **11b** showed similar racemization percentage. The major isomer was active (S), whereas the lesser isomer was inactive (R). The resulting aldehydes (**11a-b**) were then reacted with diethyl phosphite/DIPEA/DCM to yield the corresponding α-hydroxyphosphonates as a mixture of epimers (Figure 4.3). The ^{31}P NMR spectrum of compound **12b** showed the presence of two isomers in a ratio of 85.6:15.4 (Appendix C). Compound **12a,** in addition to the expected two isomers, showed two additional phosphorus-containing impurities. The desired isomer (S,S) was the major isomer present (60%).

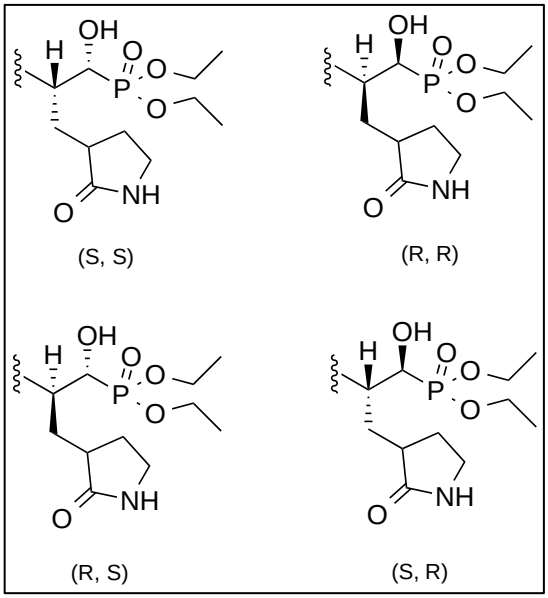

Figure 4.3 Formation of α-hydroxyphosphonate epimers.

The (S,S) isomer is the active compound.

The synthesis of dipeptide with a pyrrole functional group in the R_1 position was attempted to no avail. Pyrrole aldehyde was reacted with $NaBH_4$ in THF to yield the alcohol [64], which was reacted with the isocyanate, **6**, but the reaction was not

successful, as evidenced by the NMR spectrum. We suspected that the N-H on the pyrrole functional group interfered with the coupling of the isocyanate and alcohol. Therefore, the nitrogen on the pyrrole aldehyde was Boc-protected first [65], before reduction to alcohol, and then reaction with isocyanate. However, this method failed at the coupling of alcohol and isocyanate as well.

4.3 Biochemical studies

4.3.1 Inhibitory activity of compounds towards NoV 3CLpro

The screening results for compounds **11a-b** and **12a-b** showed promising potency against NoV. Preliminary results indicated that the transition state inhibitors (**11a-b**) possess submicromolar efficacy and the transition state mimics (**12a-b**) low micromolar values. Further experimentation determined their specific IC_{50} values to ascertain their activity against NoV. Compounds **11a-b** exhibit IC_{50} values of 0.36 µM and 0.61 µM (Table 4.1), respectively, which are indicative of favorable inhibitory activity. Compounds **12a-b**, on the other hand, display IC_{50} values of 3.51 µM and 10.8 µM, which are not as potent as compared the transition state inhibitors but are still acceptable IC_{50} values nonetheless.

Table 4.1 shows the IC_{50} values of the four compounds. It also contains two previously synthesized structures, compounds **11c** and **12c**, for the benzyl-capped aldehyde and α-hydroxyphosphonate, respectively, for ease of comparison. Compound **11c** was shown to have an IC_{50} value of 0.5 µM [40]. Compound **11a** was envisioned to interact with the 3CLpro active site by having the O in the furan acts as a hydrogen bond acceptor. It exhibits a slightly lower inhibitory activity than compound **11c**. Compound **11b** on the other hand has a slightly higher IC_{50} value. The nitrogen in the

ring was hypothesized to function as a hydrogen bond acceptor. Both compounds **11a** and **11b** did not perform as potently in the cell-based replicon system. Compound **11c** has an ED_{50} value of 0.05 M, an order of magnitude lower than that of the IC_{50}, compared to 3.5 µM and 4.1 µM of compounds **11a-b**.

Table 4.1:

In vitro and cell based inhibition of **11a-b** and **12a-b** against norovirus

Compound	Structure	IC_{50}* (µM)	ED_{50}** (µM)
11a	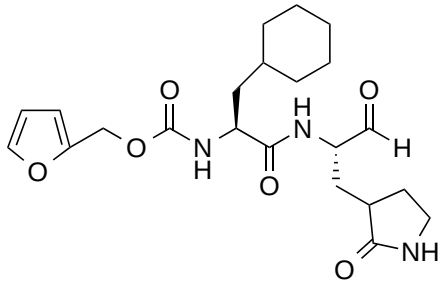	0.36	3.5
11b	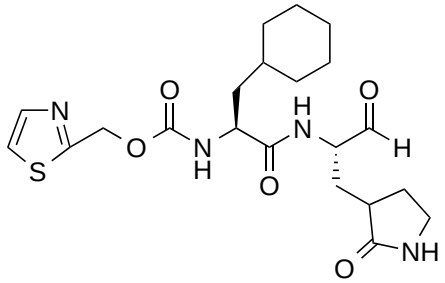	0.61	4.1
11c [40]	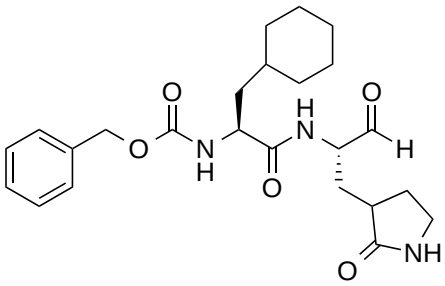	0.5	0.05

Table 4.1 (cont.)

Compound	Structure	IC_{50}* (µM)	ED_{50}** (µM)
12a* **	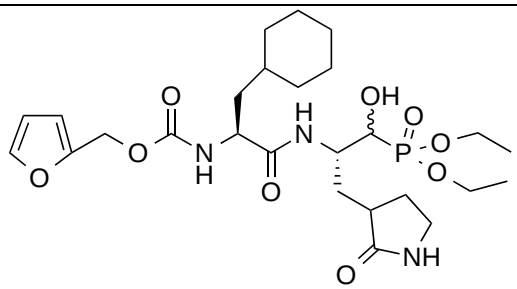	3.51	-
12b* **	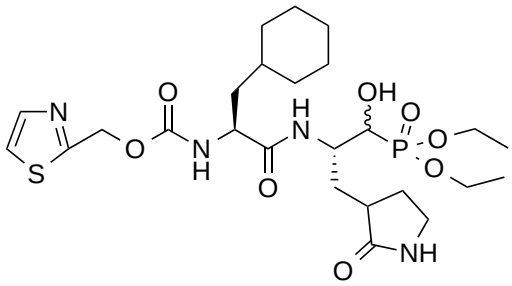	10.8	-
12c [42]	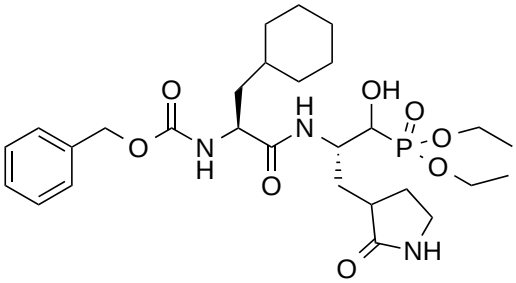	3.5	0.25

*Inhibition in vitro for NoV 3CLpro; ** Anti NoV activity in a cell-based replicon system; ***Mixture of epimers

The benzyl-capped hydroxyphosphonate, **11c**, has an IC_{50} value of 3.5 µM. Compound **11a** shows the same in vitro inhibitory activity against NoV 3CLpro as compound **11c**, whereas compound **12b** has a much lower in vitro potency. α-Hydroxyphosphonates are not as potent as aldehydes, presumably because they do not participate in covalent bond with the enzyme active site.

4.3.2 Selectivity studies

A representative panel of proteases was used to evaluate the selectivity of the inhibitors. This is of paramount importance because there is an abundance of proteases in the body; consequently toxicity may arise due to off-target effects. The selectivity profiles of compounds **11a-b** and **12a-b** are shown in Table 4.2 and 4.3 below.

Table 4.2

Selectivity of **11a-b** against a panel of proteases

Protease	Compound				$[I]_f$ (μM)
	11a		**11b**		
	I/E	% inhibition	I/E	% inhibition	
HNE	250	31	250	19	77
α-Chymotrypsin	250	0	250	0	2.5
Trypsin	250	0	250	3	125
Thrombin	250	1	250	0	2.75
Cathepsin B	5	90	5	96	0.5
Factor X_A	250	0	250	0	2.5
Plasmin	250	6	250	7	4.5
Carboxypeptidase A	250	8	250	1	43

Compounds **11a-b** exhibit fairly high selectivity against the protease panel, with the exception of the cysteine protease cathepsin B. Compounds **11a-b** inhibit cathepsin B 90 % and 96%, respectively, at an inhibitor/enzyme ratio (I/E) of 5 or a inhibitor final concentration of 0.5 µM.

Table 4.3

Selectivity of **12a-b** against a panel of proteases

Protease	Compound				$[I]_f$ (µM)
	12a		**12b**		
	I/E	% inhibition	I/E	% inhibition	
HNE	250	82	250	91	77
α-Chymotrypsin	250	0	250	0	2.5
Trypsin	250	0	250	3	125
Thrombin	250	5	250	0	2.75
Cathepsin B	5	54	5	36	0.5
Factor X_A	250	26	250	6	2.5
Plasmin	250	15	250	11	4.5
Carboxypeptidase A	250	0	250	9	43

Compounds **12a-12b** display reasonably good selectivity except against HNE and cathepsin B. Cathepsin B was inhibited at 54% and 36%, respectively, at an I/E of 5 or inhibitor final concentration of 0.5 µM. HNE was inhibited less potently than that of cathepsin B at 82% and 91%, respectively, at I/E = 250, or inhibitor final concentration of 77 µM.

The aldehydes, **11a-b**, show a better overall selectivity profile than the α-hydroxyphosphonates, **12a-b**. However, much can be learned from the observation that compounds **12a-b** show less potency against the cysteine protease cathepsin B.

In conclusion, the results of the studies described in this thesis indicate that the nature of the cap influences potency and can be used to also modulate selectivity, as well as physicochemical characteristics. More importantly, these studies provide a solid framework for advancing this series of compounds and conducting further pre-clinical studies to identify a drug candidate suitable for development.

REFERENCES

REFERENCES

[1] Scallan, E.; Hoekstra, R. M.; Angulo, F. J.; Tauxe, R. V.; Widdowson, M.-A.; Roy, S. L.; Jones, J. L.; Griffin, P. M. "Foodborne illness acquired in the US – major pathogens" *Emerg. Infect. Dis*., **2011**, 17, 7-15.

[2] Lopman, B. A.; Reacher, M. H.; Vipond, I. B.; Sarangi, J.; Brown, D. W. "Clinical manifestation of norovirus gastroenteritis in health care settings" *Clin. Infect. Dis*., **2004**, 39 (3), 318-324.

[3] Fankhauser, R. L.; Monroe, S. S.; Noel, J. S.; Humphrey, C. D.; Bresee, J. S.; Parashar, U. D.; Ando, T.; Glass, R. I.; "Epidemiologic and molecular trends of Norwalk-like viruses associated with outbreaks of fastroenteritis in the United States" *J. Infect. Dis.,* **2002**, 186, 1-7.

[4] Zheng, D.P.; Ando, T.; Fankhauser, R. L.; Beard. R. S.; Glass, R. I.; Monroe. S. S. "Norovirus classification and proposed strain nomenclature" *Virol.*, 2006, 346, 312-323.

[5] Lindesmith, L.; Moe, C.; Marionneau, S.; Ruvoen, N.; Jiang, X.; Lindblad, L.; Stewart, P.; LePendu, J.; Baric, R. "Human susceptibility and resistance to Norwalk virus infection" *Nat. Med.,* **2003**, 9 (5), 548-553.

[6] Lopman, B.; Gastanaduy, P.; Park, G. W.; Hall, A. J.; Parashar, U. D.; Vinje, J. "Environmental transmission of norovirus gastroenteritis" *Curr. Opin. Virol.* **2012**, 2, 96-102.

[7] Duizer, E.; Bijkerk, P.; Rockx, B.; De Groot, A.; Twisk, F.; Koopmans, M. "Inactivation of caliciviruses" *Appl. Environ. Microbiol.,* **2004**, 70 (8), 4538-4543.

[8] Teunis, P. F.; Moe, C. L.; Liu, P.; Miller, S. E.; Lindesmith, L.; Baric, R. S.; Le Pendu, J.; Calderon, R. L. "Norwalk virus: How infectious is it?" *J. Med. Virol.,* **2008**, 80 (8), 1468-1476.

[9] Rockx, B.; De Wit, M.; Vennema, H.; Vinje, J.; De Bruin, E.; Van Duynhoven, Y.; Koopmans, M. "Natural history of human *Calicivirus* infection: A prospective cohort study" *Clin. Infect. Dis.,* **2002**, 35 (3), 246-253.

[10] Tacket, C. O.; Sztein, M. B.; Losonsky, G. A.; Wasserman S. S.; Estes, M. K. "Humoral, mucosal, and cellular immune responses to oral Nowalk virus-like particles in volunteers" *Clin. Immunol.*, **2003**, 108 (3), 241-247.

[11] Ando, T.; Noel, J. S.; Fankhauser, R. L. "Genetic classification of Norwalk-like viruses" *J. Infect. Dis.*, **2000**, 181, S336-S348.

[12] Lay, M. K.; Atmar, R. L.; Guix, S.; Bharadwaj, U.; He, H.; Neill, F. H.; Sastry K. J.; Yao, Q.; Estes, M. K. “Norwalk virus does not replicate in human macrophages or dendritic cells derived from the peripheral blood of susceptible humans” *Virol.*, **2010**, 406, 1-11.

[13] Parrino, T. A.; Schreiber, D. S.; Trier, J. S.; Kapikian, A. Z.; Blacklow, N. R. “Clinical immunity in acute gastroenteritis caused by Norwalk agent” *N. Engl. J. Med.*, **1977**, 297 (20, 86-89.

[14] Chang, K. O.; George, D. W. “Interferons and ribavirin effectively inhibit Norwalk virus replication in replicon-bearing cells” *J. Virol.***, 2007**, 81, 12111-12118.

[15] Karst S. M.; Wobus, C. E.; Lay M.; Davidson, J.; Virgin IV, H. W. “STAT1-dependent innate immunity to a Norwalk-like virus” *Science*. **2003**, 299, 1575-1578.

[16] Duizer, E.; Schwab, K. J.; Neill, F. H.; Atmar, R. L.; Koopmans, M. P. G.; Estes, M. K. “Laboratory efforts to cultivate Noroviruses” *J. Gen. Virol.,* **2004**, 85, 79-87.

[17] Green, S. M.; Vinje, J.; Gallimore, C. I.; Koopmans, M.; Hale, A.; Brown, D. W. G.; “Capsid protein diversity among Norwalk-like viruses” *Virus Genes,* **2000**, 20, 227-236.

[18] Belliott, G.; Sosnovtsev, S. V.; Mitra, T.; Hammer, C.; Garfield, M.; Green, K. Y. “In vitro proteolytic processing of the MD145 norovirus ORF1 nonstructural polyprotein yields stable precursors and products similar to those detected in Calicivirus-infected cells” *J. Virol.*, **2003**, 77, 10957-10974.

[19] Donaldson, E. F.; Lindesmith, L. C.; Lobue, A. D.; Baric, R. S. “Viral shape-shifting: norovirus evasion of the human immune system” *Nat. Rev. Microbiol.* **2010**, 8, 231-241.

[20] Nakamura, K.; Someya, Y.; Kumasaka, T.; Ueno, G.; Yamamoto, M.; Sato, T.; Takeda, N.; Miyamura, T.; Tanaka, N. “A Norovirus protease structure provides insights into active and substrate binding site integrity” *J. Virol.*; **2005**, 79 (21), 13685-13693.

[21] Prasad, B. V.; Hardy, M. E.; Dokland, T.; Bella, J.; Rossman, M. G.; Estes, M. K. “X-ray crystallographic structure of the Norwalk virus capsid” *Science*, **1999**, 286, 287-290.

[22] Liu, B. L.; Viljoen, G. J.; Clarke, I. N.; Lambden, P. R.; “Identification of further proteolytic cleavage sites in the Southampton calicivirus polyprotein by expression of the viral protease in E. coli” *J. Gen. Virol.*, **1999**, 80, 291-296.

[23] Glass, P. J.; White, L. J.; Ball, J. M.; Leparc-Goffart, I.; Hardy, M. E.; Estes, M. K. “Norwalk virus open reading frame 3 encodes a minor structural protein” *J. Virol.*, **2000**, 74, 6581-6591.

[24] Anderson, J.; Schiffer, C.; Lee, S. K.; Swanstrom, R. “Viral protease inhibitors” *Handb. Exp. Pharmacol.*, **2009**, 85-110.

[25] Kim, Y.; Lovell, S.; Tiew, K.-C.; Mandadapu, S. R.; Alliston, K. R.; Battaile, K. P. Groutas, W. C.; Chang, K.O. “Broad-spectrum antivirals against 3C or 3C-like proteases of picornaviruses, noroviruses, and coronaviruses” *J. Virol.*, **2012**, 86 (21), 11754-11762.

[26] Hussey, R. J.; Coates, L.; Gill, R. S.; Erskine, P. T.; Coker, S.-F.; Mitchell, E.; Cooper, J. B.; Wood, S.; Broadbridge, R.; Clarke, I. N.; Lambden, P. R.; Shoolingin-Jordan, P. M.; “A structural study of Norovirus 3C protease specificity: binding of a designed active site-directed peptide inhibitor” *Biochem.,* **2011**, 50, 240-249.

[27] Schechter, I.; Berger, A. “On the size of the active site in proteases. I. Papain” *Biochem. Biophys. Res. Commun.,* **1967**, 27, 157-162.

[28] Hartley, B. S. “Proteolytic enzymes” *Annu. Rev. Biochem.*, **1960**, 29, 45-72.

[29] Rawlings, N. D. “A large and accurate collection of peptidase cleavages in the MEROPS database” *Database*, **2009**, DOI:10.1093/database/bap015

[30] Bazan, J. F.; Fletterick R. J. “Viral cysteine proteases are homologous to the trypsin-like family of serine proteases: structural and functional implications” *Proc. Natl. Acad. Sci.* **1988**, 85, 7872-7876.

[31] Dougherty, W. G.; Semler, B. L.; “Expression of virus-encoded proteinases: functional and structural similarities with cellular enzymes” *Microbiol. Rev.*, **1999**, 57, 781-822.

[32] Muhaxhiri, Z.; Deng, L.; Shanker, S.’ Sankaran, B.; Estes, M. K.; Palzkill, T.; Song, Y.; Prasad, B. V. V. “Structural basis of substrate specificity and protease inhibition in Norwalk virus” *J. Virol.*, **2013**, 87 (8), 4281-4292.

[33] Voet, D. J.; Voet, J. G.; Pratt, C. W. “Principles of Biochemistry” 3rd ed., John Wiley and Sons, Inc. **2008**, Chapter 12.

[34] Berg, J.; Tymoczko, J.; Stryer, L. “Biochemistry” 5th ed., W. H. Freeman and Company, **2002**.

[35] Pauling, L. “Chemical achievement and hope for the future” *Am. Sci.* **1948**, 36, 51-58.

[36] Chorghade, M. S. “Drug discovery and development” Volume 1., John Wiley and Sons, Inc. **2006**, pp. 2, 107.

[37] Sebaugh, J. L.; “Guidelines for accurate EC50/IC50 estimation” *Pharmaceut. Statist.*, **2011**, 10, 128-134.

[38] Takahashi, D.; Kim, Y.; Lovell, S.; Prakash, O.; Groutas, W. C.; Chang, K.-O. “Structural and inhibitor studies of norovirus 3C-like proteases” *Vir. Res.*, **2013**, 178 (2), 437-444.

[39] Prior, A. M.; Kim, Y.; Weerasekara, S.; Moroze, M.; Alliston, K. R.; Uy, R. A. Z.; Groutas, W. C.; Chang, K.-O.; Hua, D. H. “Design, synthesis, and bioevaluation of viral 3C and 3C-like protease inhibitors” *Bioorg. Med. Chem. Lett.*, **2013**, 23 (23), 6317-6320

[40] Mandadapu, S. R.; Gunnam, M. K.; Tiew, K. C.; Uy, R. A. Z.; Prior, A. M.; Alliston, K. R., Hua, D. H.; Kim, Y.; Chang, K.O.; Groutas, W. C. “Inhibition of norovirus 3CL protease by bisulfite adducts of transition state inhibitors” *Bioorg. Med. Chem. Lett.*; **2013**, 23 (1), 62-65.

[41] Mandadapu, S. R.; Weerawarna, P. W.; Prior A. M.; Uy, R. A. Z.; Aravapalli, S.; Alliston, K. R.; Lushington, G. R.; Yunjeong, K.; Duy, H. H.; Chang, K. O.; Groutas, W. C. “Macrocyclic inhibitors of 3C and 3C-like proteases of picornavirus, norovirus, and coronavirus” *Bioorg. Med. Chem. Lett.*, **2013**, 23 (13), 3709-3712.

[42] Mandadapu, S. R.; Gunnam, M. R.; Galasiti Kankanamalage, A. C.; Uy, R. A. Z.; Alliston, K. R.; Lushington, G. H.; Kim, Y.; Chang, K. O.; Groutas, W. C. “Potent inhibition of norovirus by dipeptidyl α-hydroxyphosphonate transition state mimics” *Bioorg. Med. Chem. Lett.*, **2013**, 23 (21), 5941-5944.

[43] Mandadapu, S. R.; Weerawarna, P. M.; Gunnam, M. R.; Alliston, K. R.; Lushington, G. H.; Kim, Y.; Chang, K. O.; Groutas, W. C. “Potent inhibition of norovirus 3CL protease by peptidyl α-ketoamides and α-ketoheterocycles” *Bioorg. Med. Chem. Lett.,* **2012**, 22 (14), 4820-4826.

[44] Dou, D.; Mandadapu, S. R.; Alliston, K. R.; Kim, Y.; Chang, K. O.; Groutas, W. C. “Cyclosulfamide-based derivatives as inhibitors of noroviruses” *Eur. J. Med. Chem.*, **2012**, 47 (1), 59-64.

[45] Dou, D.; He, G.; Mandadapu, S. R.; Aravapalli, S.; Kim, Y.; Chang, K. O.; Groutas, W. C. “Inhibition of noroviruses by piperazine derivatives” *Bioorg. Med. Chem. Lett.*, **2012**, 22 (1), 377-379.

[46] Dou, D.; Tiew, K. C.; Mandadapu, S. R.; Gunnam, M. R.; Alliston, K. R.; Kim, Y.; Chang, K. O.; Groutas, W. C. “Potent norovirus inhibitors based on the acyclic sulfamide scaffold” *Bioorg. Med. Chem. Lett.*, **2012**, 20 (6), 2111-2118.

[47] Dou, D.; Mandadapu, S. R.; Alliston, K. R.; Kim, Y.; Chang, K. O. ; Groutas, W. C. “Design and synthesis of inhibitors of noroviruses by scaffold hopping” *Bioorg. Med. Chem.***2011**, 19 (19), 5749-5755.

[48] Tiew, K. C.; He, G.; Aravapalli, S.; Mandadapu, S. R.; Gunnam, M. R.; Alliston, K. R.; Lushington, G. H.; Kim, Y.; Chang, K. O.; Groutas, W. C. “Design, synthesis, and evaluation of inhibitors of Norwalk virus 3C protease” *Bioorg. Med. Chem. Lett.*, **2011**, 21 (18), 5315-5319.

[49] Dou, D.; Tiew, K. C.; He, G.; Mandadapu, S. R.; Aravapalli, S.; Alliston, K. R.; Kim, Y.; Chang, K. O.; Groutas, W. C. “Potent inhibition of Norwalk virus by cyclic sulfamide derivatives” *Bioorg. Med. Chem. Lett.*, **2011**, 19(20), 5975-5983.

[50] Webber, S. E.; Okano, K.; Little, T. L.; Reich, S. H.; Xin, Y.; Fuhrman, S. A.; Matthews, D. A.; Love, R. A.; Hendrickson, T.F.; Patrick, A.K.; Meador, J. W.; Ferre, R. A.; Brown, E. L.; Ford, C. E.; Binford, S. L.; Worland, S. T. “Tripeptide Aldehyde Inhibitors of Human Rhinovirus 3C Protease: Design, Synthesis, Biological Evaluation, and Cocrystal Structure Solution of P1 Glutamine Isosteric Replacements” *J. Med. Chem.* **1998**, 41, 2786.

[51] Zeitler, C. E.; Estes, M. K.; Prasad, B. V. V. “X-ray crystallographic structure of the Norwalk virus protease at 1.5 A resolution” *J. Virol.*, **2006**, 80, 5050.

[52] Ritchie, T. J.; Ertl, P.; Lewis, R. “The graphical representation of ADME-related molecule properties for medicinal chemists” *Drug Discovery Today*, **2011**, 16, 65-72.

[53] Deng, L.; Muhaxhiri, Z.; Estes, M. K.; Palzkill, T.; Venkataram Prasad, B. V.; Song, Y. “Synthesis, activity, and structure-activity relationships of noroviral protease inhibitors” *Med. Chem. Comm.*, **2013**, 4, 1354-1359.

[54] Mou, X.; Xu, B.; Ma, C.; Yang, X.; Zou, X.; Lu, Y.; Xu, P. “Novel CADD-based peptidyl vinyl ester derivatives as potential proteasome inhibitors” *Bioorg. Med. Chem. Lett.*, **2008**, 18, 2198-2202.

[55] Chang, K.-O.; Takahashi, D.; Prakash, O.; Kim, Y. “Characterization and inhibition of norovirus proteases of genogroups I and II using a fluorescence resonance energy transfer assay” *Virol.* **2012**, 423, 125-133.

[56] Wei, L.; Zhong, J.; Gan, X.; Alliston, K. R.; Groutas, W. C. “Design, synthesis, and in vitro evaluation of inhibitors of human leukocyte elastase based on a functionalized cyclic sulfamide scaffold” *Bioorg. Med. Chem.*, **2003**, 12, 589-593.

[57] Kay, G.; Bailie, J. R.; Halliday, I. M.; Nelson, J.; Walker, B. “The synthesis, kinetic characterization, and application of biotinylated aminoacylchloromethanes for the detection of chymotrypsin and trypsin-like serine proteases” *Biochem. J.* **1992**, 283, 455-459.

[58] Di Fenza, A.; Heine, A.; Koert, U.; Klebe, G. “Understanding the binding selectivity toward Trypsin and Factor Xa: the role of aromatic interactions” *Chem. Med. Chem.* **2007**, 2, 297-308.

[59] Sidhu, P. S.; Liang, A.; Mehta, A. Y.; Abdel Aziz, M. H.; Zhou, Q.; Desai, U. R. “Rational design of potent, small, synthetic allosteric inhibitors of Thrombin” *J. Med. Chem.* **2011**, 54, 5522-5531.

[60] Taggart, C.C.; Lowe, G. J.; Greene, C. M.; Mulgrew, A. T.; O’Neill, S. J.; Levine, R. L.; McElvaney, N. G. “Cathepsin B, L, and S cleave and inactivate secretory leucoprotease inhibitor” *J. Biol. Chem.* **2001**, 276, 33345-33352.

[61] Hopfner, K. P.; Brandstetter, H.; Karcher, A.; Kopetzki, E.; Huber, R.; Engh, R. A.; Bode, W. “Converting blood coagulation factor IXa into factor Xa: dramatic increase in amidolytic activity identifies important active site determinants” *EMBO J.* **1997**, 16, 6626-6635.

[62] Yang, H.; Wang, Y.; Xiao, Y, Wang, Y.; Wu, J.; Liu, C.; Ye, H.; Li, F.; Yu, H.; Lai, R. “A bi-functional anti-thrombosis protein containing both direct-acting fibrin(ogen)olytic and plasminogen-activating activities” *PLoS One*, **2011**, 6, (3), 1-12.

[63] Payne, D. J.; Bateson, J. H.; Tolson, D.; Gasson, B. Khushi, T.; Ledent, P.; Frere, J.-M. “Phosphonamidate analogues of dipeptides with carboxypeptidase A and β-lactamase- inhibitory activity: elucidation of the mechanism of β-lactamase inhibition by electrospray mass spectrometry” *Biochem. J.* **1996**, 314, 457-461.

[64] Ryppa, C.;Senge, M. O.; Hatscher, S. S.; Kleinpeter, E.; Wacker, P.; Schilde, U.; Wiehe, A. “Synthesis of mono- and disubstituted porphyrins: A- and 5,10-A2-Type systems” *Chem. Eur. J.* **2005**, 11, 3427-3442.

[65] Handy, S. T.; Sabatini, J. J.; Zhang, Y.; Vulfova, I. “Protection of poorly nucleophilic pyrroles” *Tet. Lett.* **2004**, 45, 5057-5060.

APPENDICES

APPENDIX A

SIGMOIDAL PLOTS FOR IC_{50} DETERMINATION

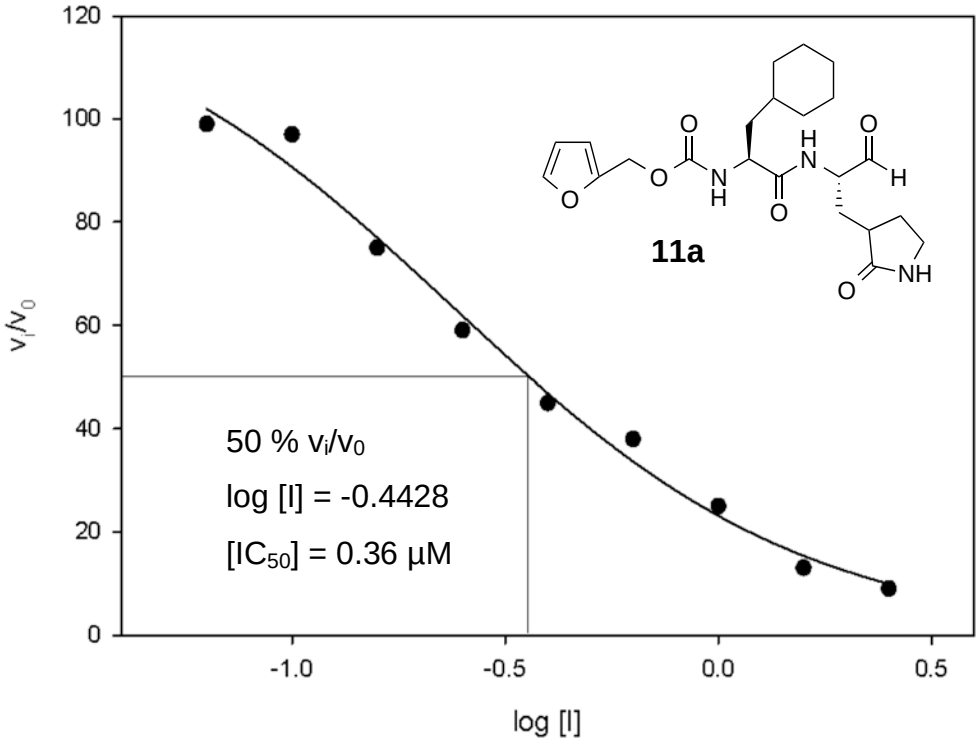

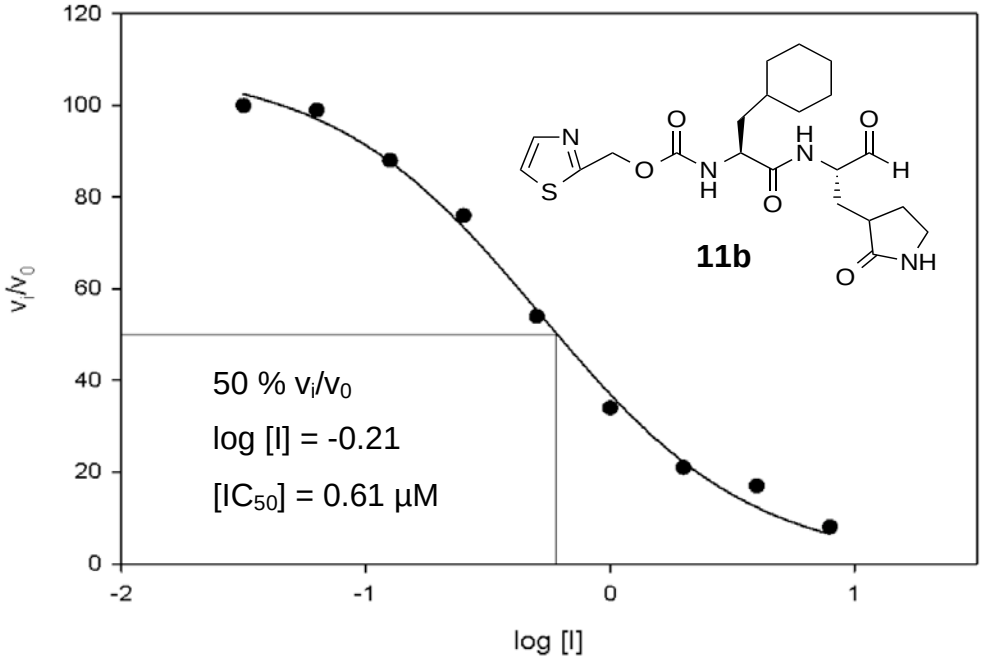

APPENDIX A (cont.)

SIGMOIDAL PLOTS FOR IC_{50} DETERMINATION

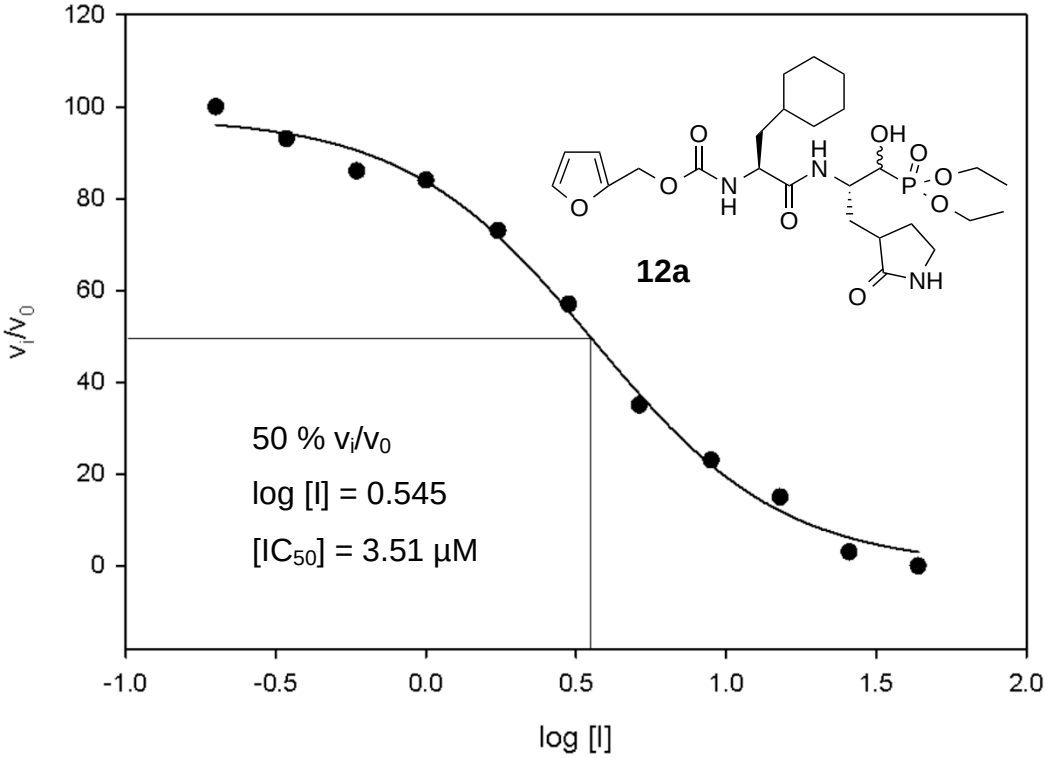

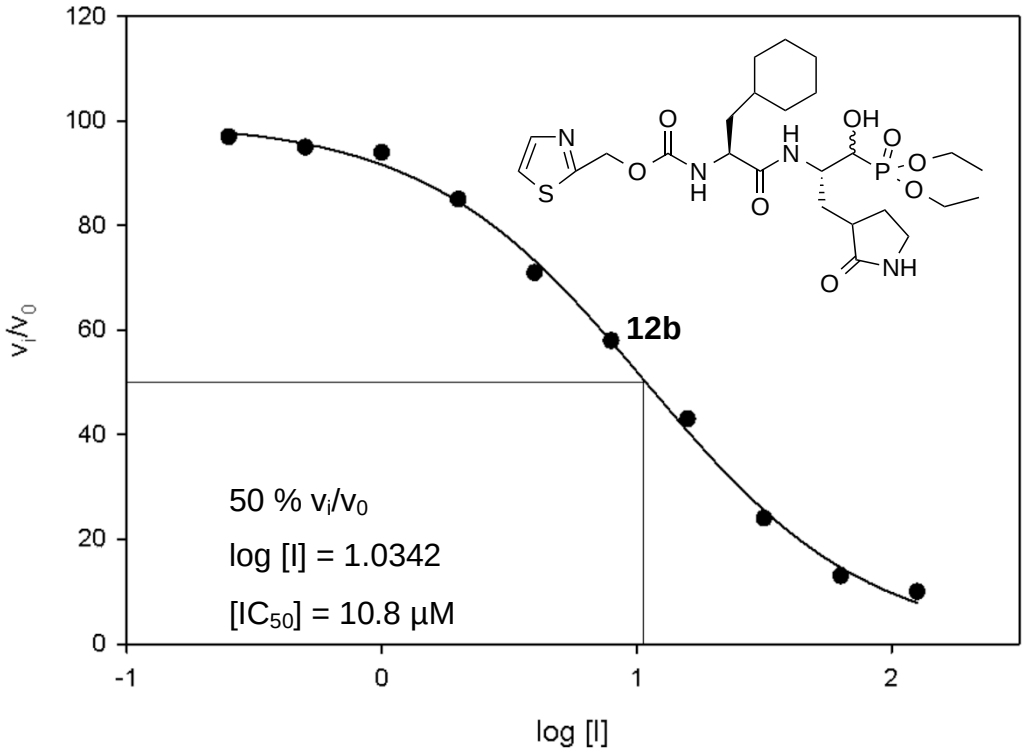

APPENDIX B

^{1}H NMR spectra for compounds **11a-b**

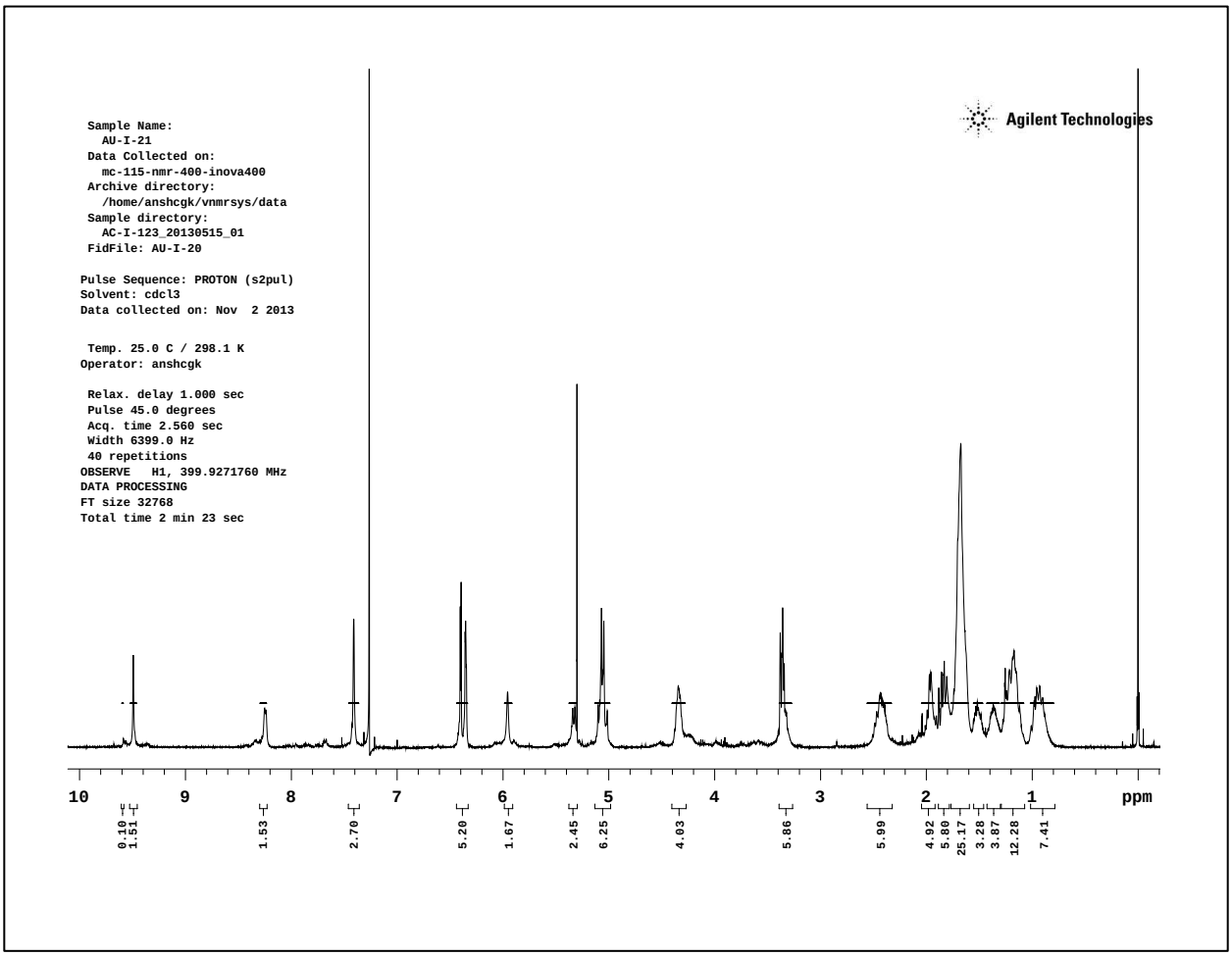

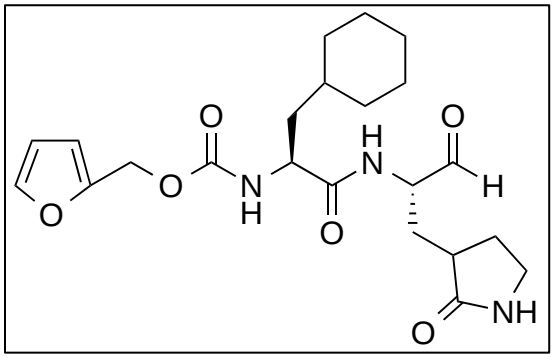

11a

APPENDIX B (cont.)

^{1}H NMR spectra for compounds **11a-b**

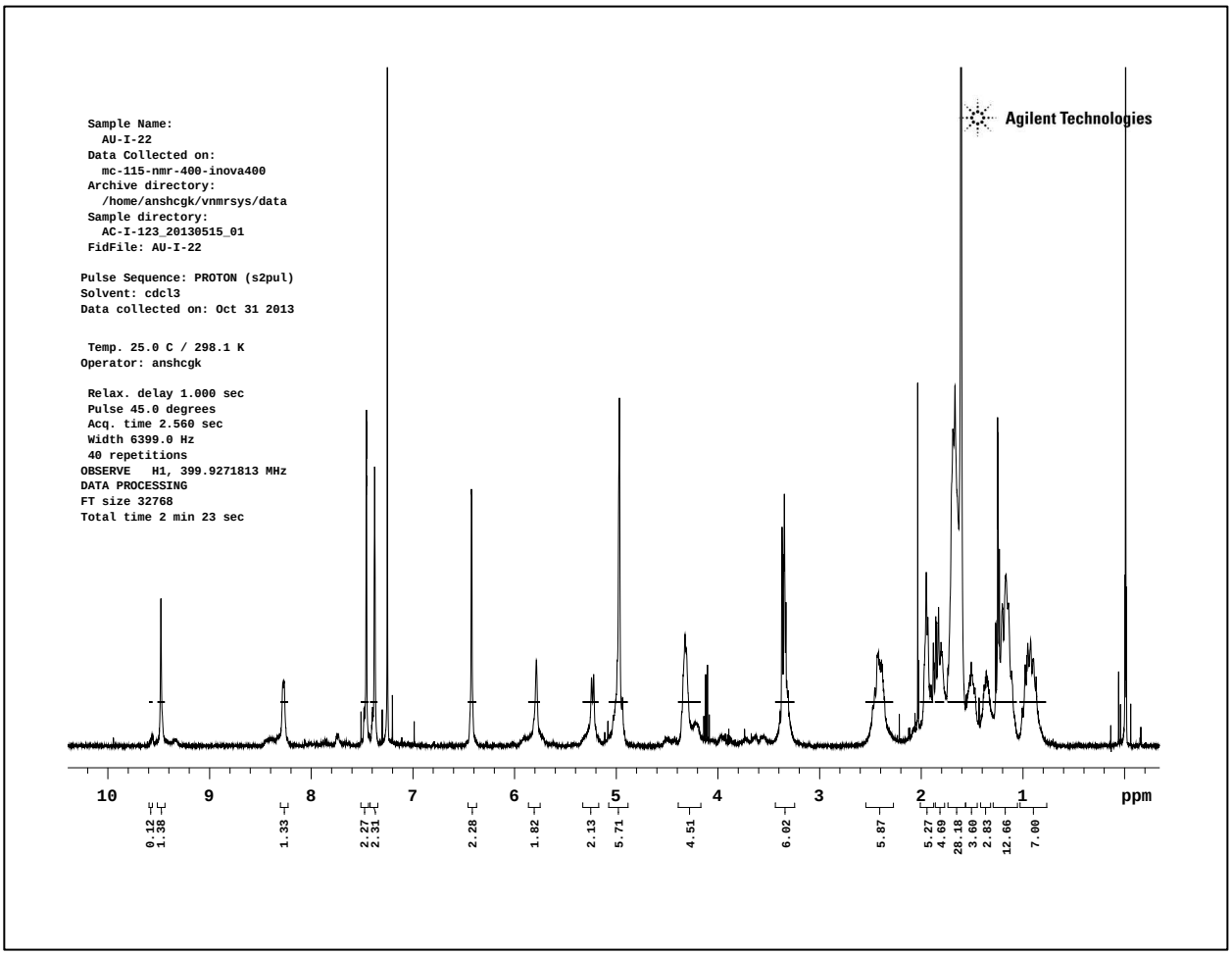

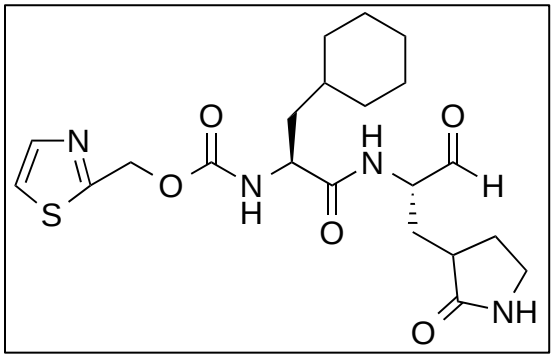

11b

APPENDIX C

^{31}P NMR spectra for compounds **12a-b**

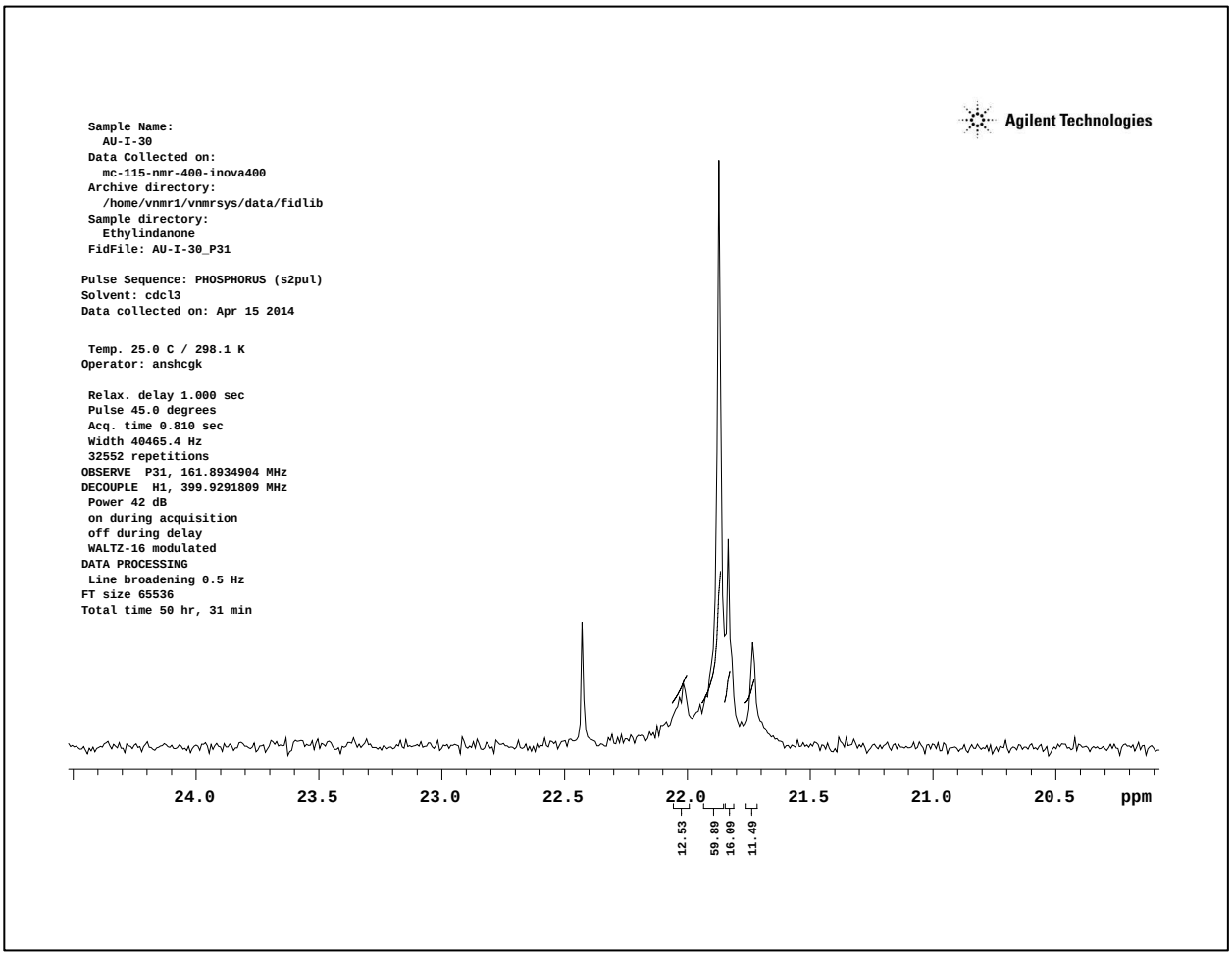

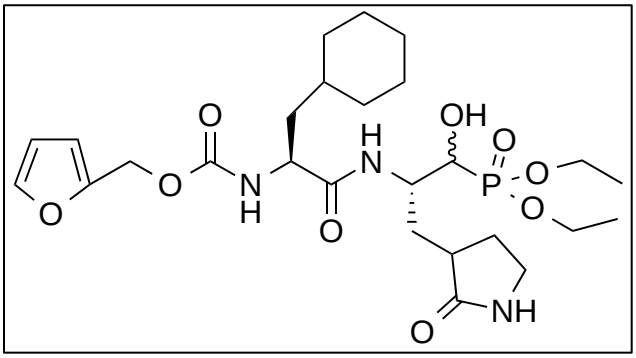

12a

APPENDIX C (cont.)

^{31}P NMR spectra for compounds **12a-b**

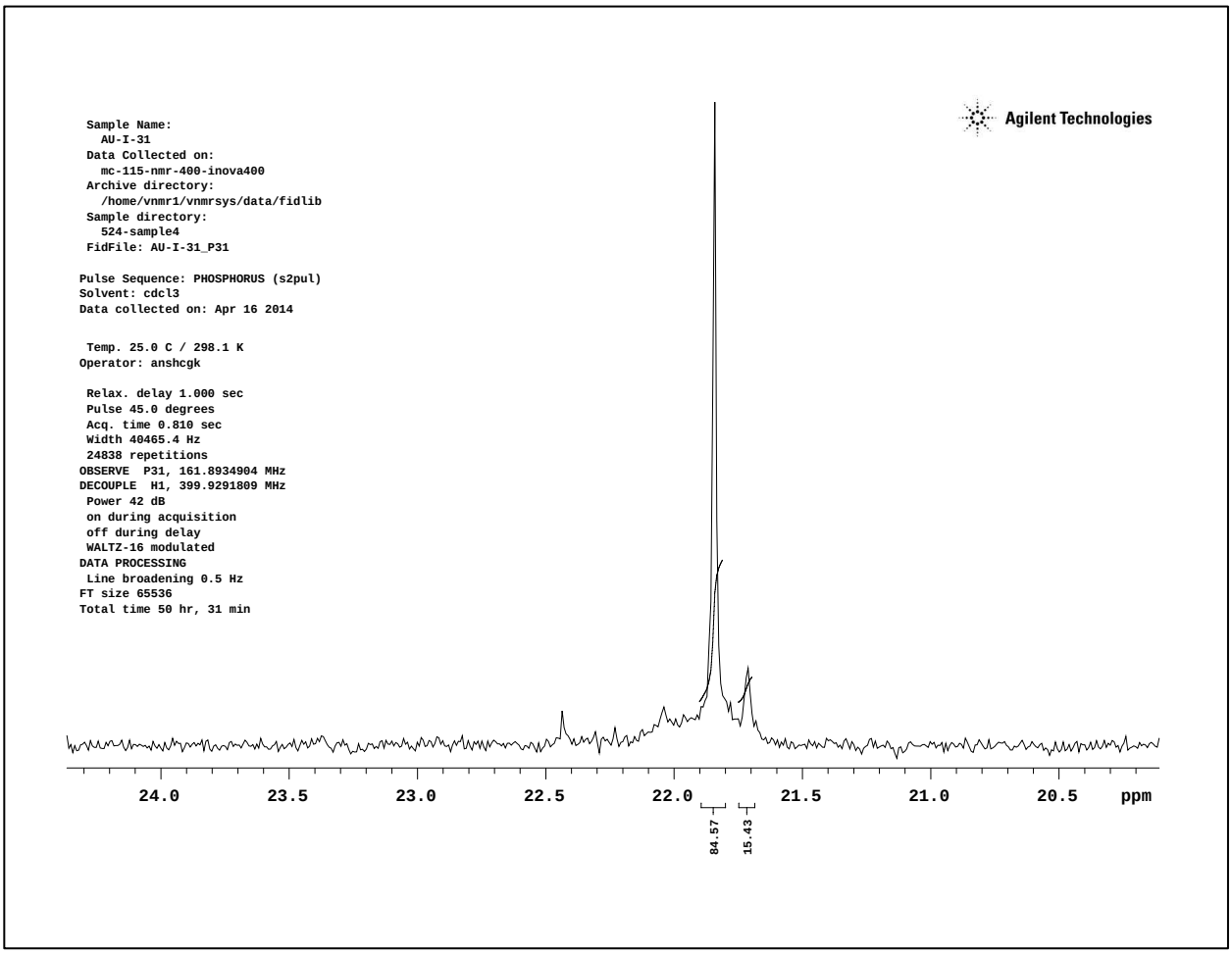

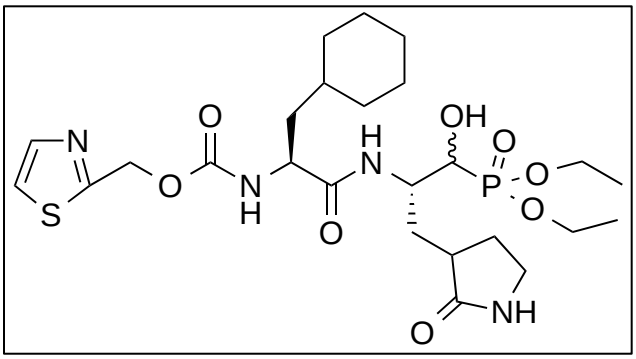

12b